Graphite Nanoplatelet Filler-Modified Polyurethane Nanocomposites for Thermal Transport Enhancement

by

Usama Akram

A thesis submitted in partial fulfillment of the requirements for the degree of

Master of Science

Department of Mechanical Engineering
University of Alberta

ABSTRACT

The use of polymers in applications such as electronic packaging, heat exchangers, and thermal pastes is limited by their inability to dissipate accumulated heat effectively. Nano-scale filler modifiers may be used to improve the transport of thermal energy through polymer materials. Studies of thermally-enhanced polymer nanocomposites have shown minimal enhancement by filler addition due to the presence of an interfacial or Kapitza resistance caused by phonon mismatch. In this study, a graphite nanoplatelet (GNP) filler modifier was added to polyurethane (PU) that is typically used in high wear applications. Due to PU's low thermal conductivity of 0.2 W/m-K, accumulated heat can cause degradation and early failure. A specialized curing chamber, allowing for the application of heat and high vacuum pressure was used to produce high quality nanocomposite specimens with minimal void content. GNP-PU specimens modified with up to 4% GNP filler weight content were produced through solution blending. X-Ray Diffraction (XRD) analysis performed on the specimens to investigate filler dispersion suggested that no intercalation or exfoliation of the nanofillers had occurred. The bulk thermal conductivity of the filler-modified PU specimens was tested using the hot disk method. A linear enhancement trend, reaching a maximum bulk conductivity value of 0.43 W/m-K, with no percolating behavior, was observed for the thermal conductivity of the GNP-PU modified nanocomposite. These experimental values were found upon comparison to be in agreement with results of second-order analytical models based on the series model. Differential scanning calorimetry (DSC) was performed to measure the specific heat capacity of the test specimens for anisotropic hot disk testing. Results of anisotropic hot disk testing showed a higher in-plane thermal conductivity value as compared to thermal conductivity in the through-thickness direction in all modified specimens. Further compression testing and hot disk analysis at various

probing depths suggested filler alignment in the in-plane direction as well as GNP settlement at the base of the nanocomposite specimens.

TABLE OF CONTENTS

LIST OF FIGURES

LIST OF TABLES

NOMENCLATURE AND ABBREVIATIONS

i. Symbols

A	temperature Coefficient of Resistivity (Ω/°K)
C_p	specific heat capacity (J/kgK)
$D(\tau)$	dimensionless time-dependent function
d_{hkl}	distance by which planes hkl are separated (m)
k	thermal conductivity (W/m-K)
M	dimensionless shape factor
N	dimensionless shape factor
n	order of diffraction signal
P	total power output from sensor (W)
Q	heat flux (W)
r	filler radius (m)
r_s	sensor disk radius (m)
R	thermal resistance (°K/W)
$R(t)$	hot disk resistance as a function of time (Ω)
R_0	disk resistance at t=0 (Ω)
s	filler thickness (m)
SA	surface area (m^2)
ΔT	temperature gradient (°K)
$\Delta T_{AVG}(\tau)$	temperature increase of specimen surface (°K)
ΔT_i	constant temperature difference between surfaces where $\Delta T_i = 0$ in perfect sensor-specimen contact (°K)
t	time measured from start of transient recording (s)

Δt_i	short time period in which ΔT_i becomes constant (s)
V	volume (m3)
W	weight (kg)
x	length (m)

ii. Greek Symbols

α	specimen thermal diffusivity (m2/s)
α_i	Kapton insulation layer diffusivity (m2/s)
θ	diffraction angle (°)
λ	wavelength of impinging X-Ray beam (m)
ξ	Kapton insulation layer thickness (m)
ρ	density (kg/m3)
π	3.14159265359

iii. Subscripts

a	through-thickness
r	in-plane
nc	nanocomposite
f	filler
m	matrix

iv. Abbreviations

GNP	Graphite Nanoplatelets
PU	Polyurethane polymer
XRD	X-Ray Diffraction
TPS	Transient Plane Source
DSC	Differential Scanning Calorimetry

FRPC	Fiber Reinforced Polymer Composites
PMC	Polymer Matrix Composites
FVF	Fiber (or filler) Volume Fraction
FWF	Fiber (or filler) Weight Fraction
CNT	Carbon Nanotubes
MEK	Methyl Ethyl Ketone
WAXD	Wide Angle X-Ray Diffraction

1. INTRODUCTION

1.1 POLYMER MATERIALS

Among engineering materials, polymers (or plastics) are considered comparatively complex due to the nature of their chemical structure, which is composed of macromolecular chains [1] [2] [3] [4]. Covalent bonds within the macromolecules fix the atoms in place, while the chain links are connected through temperature dependent dipoles, hydrogen bonds, and van der Waals bonds [1] [2] [3] [4]. Organic units known as monomers are linked (or polymerized) to form these macromolecules [1] [2] [3] [4]. The polymerization reaction may be one of addition (chain-growth) or condensation (step-growth), and involves the stages of chain initiation, propagation, and termination [5] [6] [3]. Chain molecules may be linear or branched with the addition of side chains [5] [2]. The degree of polymerization in a polymer is determined by the average number of monomer units in a chain molecule [1] [2] [3] [4]. Since it is possible to use any molecule compatible with this chain linking method to synthesise polymers, a great degree of physical and chemical properties have been achieved through polymers since the 1920s [1] [5] [2] [3] [7] [4].

The mobility of the chain molecules at any time determines the mechanical properties of a polymer [1] [8]. Polymers such as elastomers or thermosets consist of cross-linked chains, as shown in Fig. 1, bonded by covalent bonds. As a result of these cross-links, the chains are fixed more rigidly relative to one another [1] [2] [9]. Highly cross-linked polymers are brittle while materials with little or no cross-linking are elastic [9]. Unlike ceramics and metals, it is very difficult to achieve a regular (crystalline) internal structure in a polymer due to the length of the polymer chain units [1] [2] [8]. The chains will instead become twisted and entangled, which will result in a partially amorphous structure at a minimum [1] [2] [8]. Thermoplastic polymers, which cannot be cross-linked, are said to have a high degree of crystallinity (semi-crystalline) [1]. Polymers with minimal side-chains (branching) will also be more likely to form crystalline regions [5].

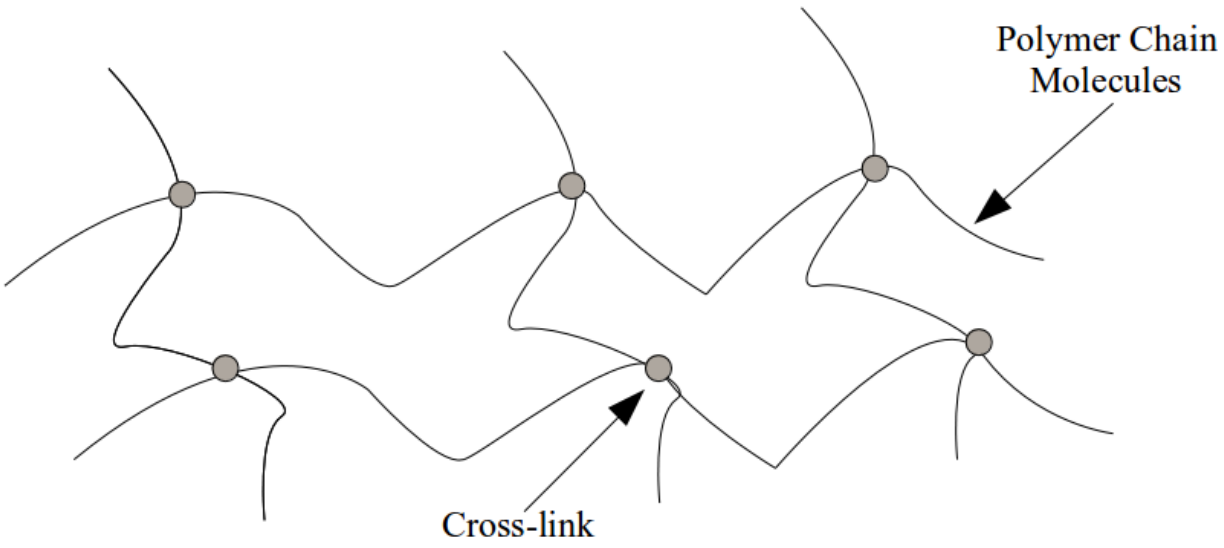

Figure 1 Cross-links between chain molecules (adapted from *[2]*)

At elevated temperatures, and owing to the increased energy, the inter-chain bonding becomes weakened and chain mobility is increased. This is known as relaxation [5] [4]. Depending on the chemical structure of the material, a number of relaxation mechanisms may come into play at varying temperatures [5] [4]. In amorphous regions, at a sufficiently high temperature, marked by a significant increase in the thermal expansion of a polymer (i. e. the rate of increase in volume per unit °Kelvin) as shown in Fig. 2, it becomes possible for the molecules to rearrange themselves in the absence of an external stress. This is known as the glass transition temperature (typically approximately 60% of the melting temperature and measured in °Kelvin) [5] [8] [4]. This results in a ductile, but solid material [5] [8] [4]. Elastomers are used above the glass transition temperature as they are highly elastic in this range [5] [2] [4].

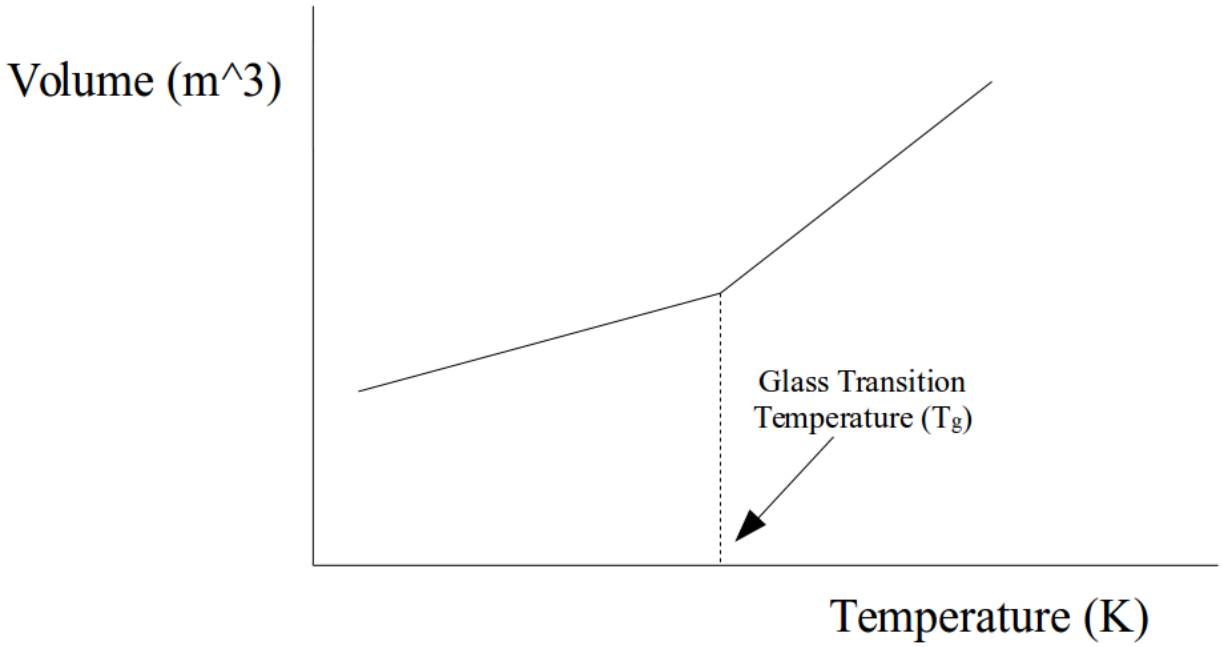

Figure 2 Glass transition, characterised by rapid increase in thermal expansion (adapted from *[8]*)

Crystalline regions, in semi-crystalline polymers, will become liquid at the melting temperature [5] [9] [4]. In thermoplastics, this melting is reversible and the material will stiffen upon cooling [2] [3] [9]. However, melting does not occur in cross-linked polymers due to the nature of the covalent bonds present in the chain molecules, which prevent the molecules from disengaging entirely with the network. At a sufficiently high temperature, irreversible decomposition will instead occur [5] [2] [3] [9]. Materials with a lower degree of polymerization (molecular weight) will have lower melting and glass transition temperatures [5]. A polymer's degree of polymerization also influences its strength, plasticity, elasticity, and viscosity [5] [2] [4] [10] [11].

Owing to the large spectrum of properties that can be achieved, polymer materials have a number of varied applications including furniture, packaging, construction, aerospace, chemical, and transportation [5] [2]. Specialty polymers such as polysulfone and PTFE may be used in high temperature and fire-resistance applications, respectively [12] [13]. In medicine, biocompatible polymers have been developed for use in applications such as pacemakers, blood bags, and replacement joints [2] [14] [15]. Liquid crystalline polymers may be used in electrical components, fiber optics, surgical instruments, and chemical equipment by virtue of their

superior mechanical and barrier properties [12]. Although polymers have typically been used as electrical insulators, due to their low conductivity, developments in polymer synthesis have allowed the introduction of materials (such as doped poly(acetylene) and Poly(pyrrole)) possessing electrical conductivity values comparable to those of metals [14] [12]. Shape memory polymers, such as segmented polyurethanes, possess the ability to return to their original shape after deformation, due to temperature changes [12].

1.2 COMPOSITE MATERIALS

Composite (or macrocomposite) materials, such as metal matrix or ceramic matrix composites, consist of two distinct non-dissolving phases (Fig. 3), combined with one another to achieve superior properties over the individual constituent phases (e. g. wood, concrete, and fibreglass) [16] [17] [18] [19]. Fiber reinforced polymer composites (FRPC) or polymer matrix composites (PMC) consist of a polymer (matrix or continuous) phase and a reinforcing (dispersed) phase of highly engineered low defect, high aspect ratio fibers, flakes, or laminates [20] [18] [21] [22] [19] [2]. These materials offer substantial advantages in specific properties such as strength and stiffness. This has resulted in their competitive use in lightweight applications for over seventy years [23] [24] [25] [26] [27] [2] [28]. High resistance to abrasion, corrosion, and fracture are also found in polymer composites [24] [25] [29] [2]. PMCs offer economic advantages due to their ease of fabrication and low material costs [16] [25].

PMCs are used extensively in aerospace applications, due to their high specific properties which result in lower weights and fuel costs, as well as the marine, civil, mining, construction, electrical, energy, and automotive industries [17] [24] [29] [18] [30] [28]. Some of the more novel applications for PMCs include bulletproof vests, medical implants and prosthetics, and structural repair [31] [32] [33] [34]. Polymers that may be utilised as PMC matrix materials include epoxy, polyamide, and polyester [29] [27] [22] [19]. Polymer matrices are low weight, low cost, easy to process, and resistant to chemical damage. However, they are also limited by inferior mechanical and thermal properties [19] [2] [12] [35]. Carbon (or graphite), glass, and Kevlar fibers are the most common reinforcing materials [20] [29] [27] [22] [19].

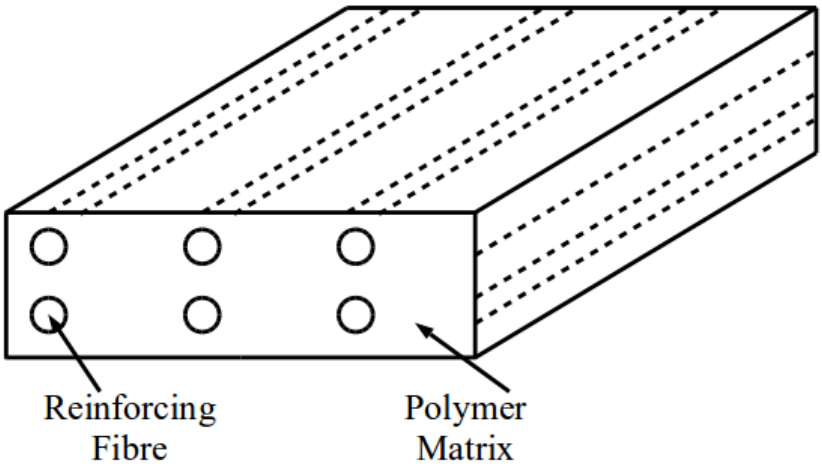

Figure 3 Polymer matrix reinforced by highly engineered fibers (exaggerated scale)

Multiple (or hybrid) reinforcing fibers may be added to polymers in certain applications (e. g. glass and carbon fibers) to create novel macrocomposite materials [31] [32] [36]. Microcomposites involve the use of micro-scale particulate fillers such as carbon black, which may be used as reinforcements in applications such as natural rubber in tyres [17] [34] [37]. Additionally, nanofillers may be added to polymers to develop novel, multifunctional materials (Fig. 4) possessing a number of unique properties, such as impermeability, improved fracture toughness, temperature stability, and emission control. Fillers such as clay, mica, and graphene may be used in polymer nanocomposites [23] [17] [18] [2]. Such nanofillers may also be used in addition to reinforcing particles or fibers to create materials with superior mechanical and multifunctional properties, e. g. structural materials capable of conducting electricity [18] [38] [39] [37].

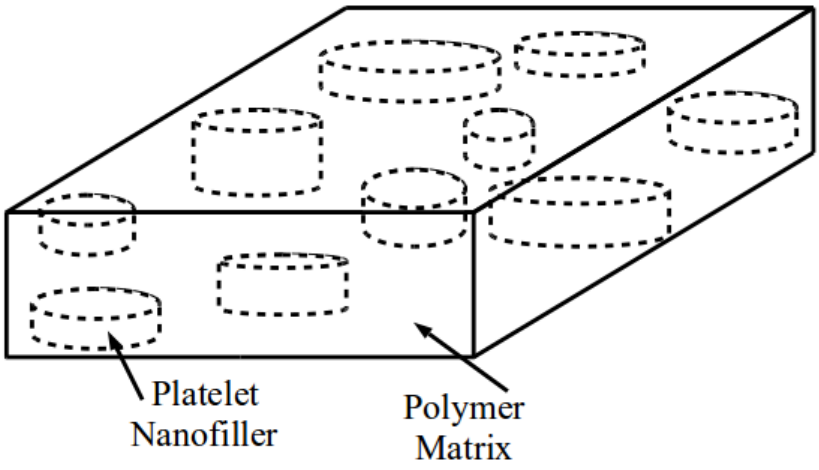

Figure 4 Polymer matrix reinforced by highly engineered nano-scale filler modifiers (exaggerated scale)

The development of novel polymers, reinforcing materials, and fabrication techniques for superior performance and longevity of composite parts continues [16] [2]. Recyclability and biodegradability are also being researched to develop sustainable, green composites [16] [27] [21] [40] [41]. Studies on composite interfacial interaction are expected to yield new characterization techniques and superior materials for long-term use [16] [42].

1.3 POLYURETHANE

Polyurethanes (PU) are an organic group of thermoset and thermoplastic polymer materials used in a number of industries including the electrical, chemical, biomedical, automotive, and mining [43] [44] [45]. Initially developed during the 1930s by Otto Bayer and his team at I. G. Farben in Leverkusen, Germany, as rubber substitutes, the materials found major use as foams and coatings during World War II [46] [47] [48] [49] [9] [7]. The first set of commercial PUs were produced in the 1950s and development has continued since to produce materials with superior properties in load-bearing, toughness, adhesion, and chemical, ozone, cut, and tear resistance, as well as advantages in cost, and energy savings [46] [50] [51] [52] [53] [9] [7]. Through variations in chemistry, particularly in the type and degree of cross-linking or branching, several families of PU materials have been developed. This has allowed for their use in a wide variety of applications [54] [47] [45] [55]. The advancement and increasing use of naturally occurring renewable monomers has reduced the environmental impact and the dependence on fossil fuels involved in the production and use of PU materials [56] [55] [57] [58]. PU may also be used as a matrix material in a number of composite applications due to its high toughness, quick fabrication process, and superior durability [25] [7] [58].

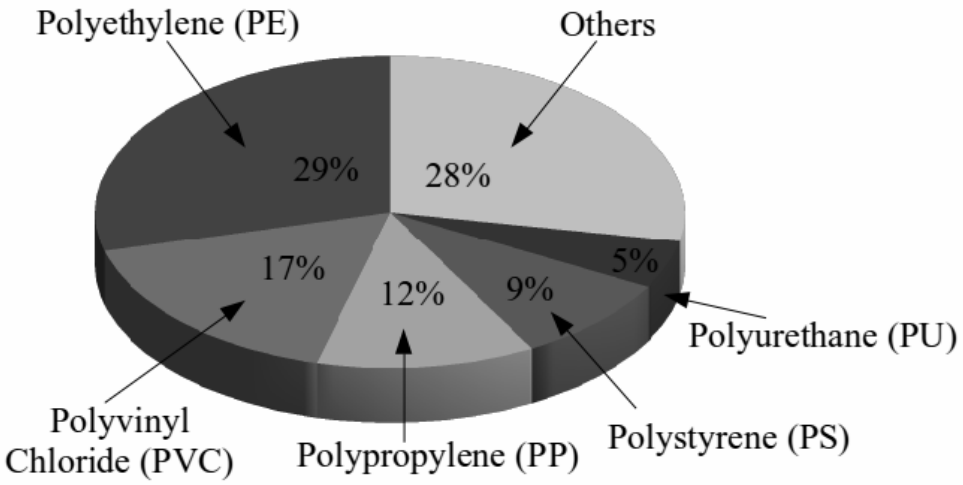

Figure 5 Polymer market (1990) (adapted from *[47]*)

Polyurethane materials, named for the urethane group illustrated in Fig. 6, consist of three main building blocks: the polyol, the isocyanate, and the curative/chain extender [59] [60] [61] [62] [56] [55] [57] [3] [7]. Polyols, which form the backbone of the PU, introduce flexibility – the two main types of polyols are polyethers and polyesters [47] [63] [60] [61] [62] [3] [7]. Polyether-based polyurethanes have lower strength and toughness, but are more hydrolytically stable [54] [62]. The hard phase of the PU consists of the isocyanate [54] [47] [64]. There are three main isocyanate materials used to synthesize castable PUs: 2,4-Toluene diisocyanate (TDI), Diphenylmethane-4,4′-diisocyanate (MDI), and Naphthalene diisocyanate (NDI) [47] [63] [60] [61] [62] [7]. Chain extenders are mainly hydroxyls and diamines [54] [63] [60] [61]. The final properties of the polymer will depend on these constituent elements and its processing conditions [65] [45] [66].

As engineering materials, PUs offer competitive performance in applications conventionally fulfilled by metals, rubbers, and other plastics. In comparison to metals, the primary benefits of PUs include their lower density, easier fabrication of complex shapes, lower energy and labor input, superior chemical resistance and wear resistance, and the ability to elastically deform to allow movement of parts [67] [45] [66] [53]. The resilience of PU can also offer energy-absorption and noise-reduction but heat buildup can lead to issues [67]. PU property emulation may be achieved through extensive rubber modification. However, rubber processing is costlier and yields inferior load-bearing properties [67] [51] [66]. In comparison to other polymers, the production of thicker cross-sections with minimal machining and lower tooling costs, are the main benefits of PU. Higher resilience, wear resistance, and radiation resistance, also improve their competitiveness in certain applications [67] [45] [66].

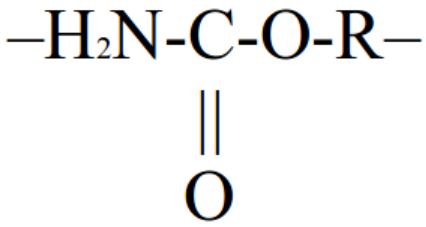

Figure 6 Basic urethane (adapted from *[47]*)

The application of PU, however, is limited by a number of factors such as exposure to high temperatures, which can lead to thermal-oxidation aging [44] [50] [68] [69] [45] [64] [55] [53]. Depending on the makeup of the material the normal temperature range may span between ambient conditions to 120°C [65] [67] [45] [53]. At lower temperatures, the material will become hard and glassy while at higher temperatures, softening and eventually, irreversible breakdown of properties, will occur beginning with the melting of the internal section of the part [65]. Thermal aging also becomes an issue at temperatures higher than 80°C [65] [68]. Additionally, the mechanical properties and performance of PU are highly temperature dependant [70] [71]. While a major material benefit in dynamic and wear-resisting applications, PU resilience results in the build-up of heat due to energy absorption [65] [67]. Failure to efficiently remove this heat can result in overheating and eventual part failure [67].

The rate of heat flow in a body depends on its geometry, the temperature gradient present, and a temperature-dependant material property known as its thermal conductivity [72]. As polyurethane has a comparatively low thermal conductivity – typically in the order of 0.1-0.3 W/m-K – the dissipation of heat caused by energy absorption can be a significant issue in application [44] [65] [67]. Reducing the cross-section of the part as well as providing a heat-sink, such as a metallic contact surface, can help minimize the potential risk of failure due to heat build-up [65] [67]. An appropriate lubricant may also be applied to reduce the build-up of heat due to friction [65].

1.3.1 POLYURETHANE APPLICATIONS

Under the CASE (Coatings, Adhesives, Sealants, and Elastomers) designation used to classify polymers, PU has applications in all four categories, as well as flexible and rigid foams [66] [55] [57] [9] [7]. Flexible foams may be used as cushioning in furniture, automotive seating, and beddings, while rigid foams are used as insulation in buildings and appliances [66] [56] [9] [7]. PU coatings are used primarily for their properties in chemical and abrasion resistance [73] [62] [7]. Their applications include the automotive, textile, and construction industries [46] [51] [66]. The toughness, strength, lower processing costs, flexibility, and low temperature performance of PUs also makes them superior adhesives [73] [52] [62]. Applications can include textiles, footwear, construction, transportation, and furniture [52] [66] [7]. PU sealants offer

excellent long-term moisture barrier properties and may be used in elevator wells, patios, and planter boxes [73].

PU elastomers include a number of groups such as millable polyurethanes, foams, thermoplastic polyurethanes, and castable polyurethane elastomers [73]. These materials are among the largest applications of polyurethane in domestic and industrial environments, being used as footwear, engine mounts, wheels, pump and pipe liners (Fig. 8) and seals, rocket coatings, sonar windows, etc. [73] [66] [74] [75] [7]. Their benefits include high modulus, elasticity, resistance to chemical and abrasion damage, low temperature performance, biocompatibility, and tailorability [76] [74] [75]. PU elastomers also allow for easy prototyping and short production runs [73].

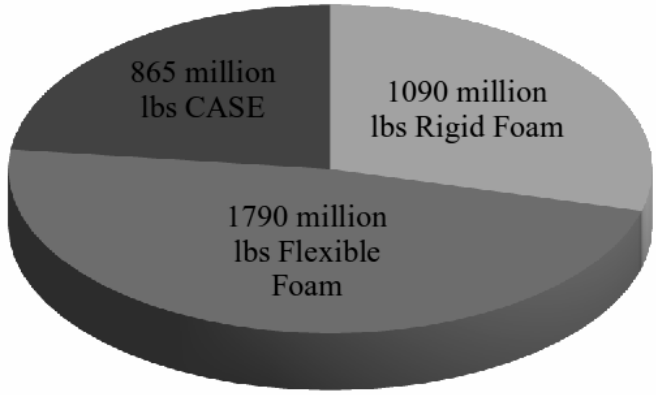

Figure 7 US Polyurethane consumption (1993) (adapted from *[66]*)

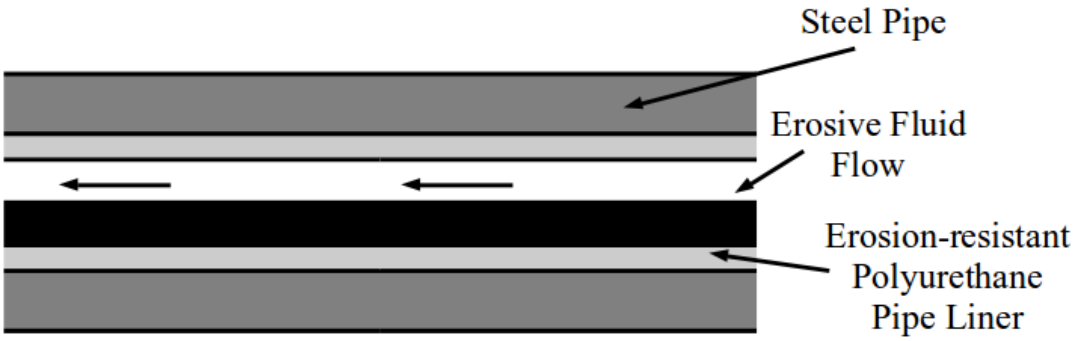

Figure 8 Polyurethane pipe liner applied to steel pipe under erosive wear

1.4 POLYMER NANOCOMPOSITES

As in the case of macrocomposites, surface interaction between the reinforcement and matrix phases determines the extent of property transfer and enhancement in polymer nanocomposites [77] [78] [79] [80] [81]. These filler modifiers may be characterized as having at least one dimension in the nano-scale, and thus as illustrated in Fig. 9, high surface areas per unit volume as compared to macro- or micro-scale reinforcing materials [82] [83] [84] [85] [86] [41] [87] [88]. As a result, the area of interaction between the phases is significantly increased, which allows high property enhancement at very low filler volume fractions [82] [89] [90] [91] [92] [15] [93] [85] [87] [37]. Polymers may therefore be improved substantially without a significant change in density or appearance [94] [77] [85]. In addition to the improvement of mechanical properties such as tensile strength, toughness, modulus, and abrasion resistance, these nano-scale filler modifiers also provide access to novel properties such as enhanced gas permeability, electrical conductivity, thermal stability, bacterial-resistance, dielectric permittivity, self-repair, and flame retardation [82] [89] [39] [90] [84] [92] [15] [41] [93] [79] [28] [81].

Other factors that may influence phase interaction, and hence property improvement, include filler dispersion and distribution, degree of agglomeration, filler volume fraction, particle shape, particle size, particle orientation, and surface adhesion [82] [89] [91] [84] [95] [85] [86]. As shown in Fig. 10, fillers are said to be fully distributed if the reinforcing particles are divided evenly in the matrix phase. Fully dispersed fillers are fully de-agglomerated (or exfoliated) particles in the matrix phase [90] [95] [79]. Perfect filler distribution ensures homogenous property enhancement throughout the matrix phase, while perfect exfoliation or dispersion of fillers ensures maximum surface interaction and property enhancement [35] [96] [91] [92] [15] [97] [98] [99] [100] [80] [101]. Due to the presence of intermolecular van der Waals forces, filler particles have a tendency to aggregate into bundles or clumps within the polymer phase [96] [90] [91] [78] [95] [97] [99] [93] [80] [101]. These particle agglomerates are typically considered problematic as they can reduce the surface interaction between the phases and also cause macrophase separation, resulting in reduced enhancement or even property degradation of the continuous phase [96] [90] [97] [93] [100] [101].

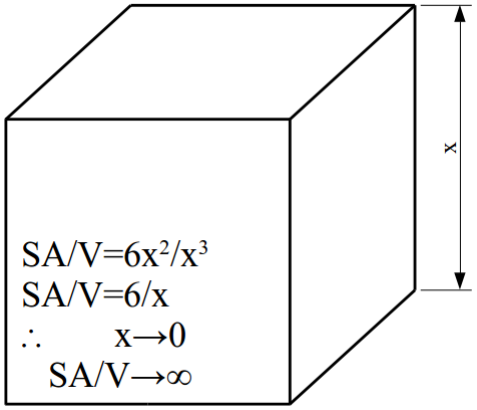

Figure 9 Effect of size reduction on surface area per unit volume

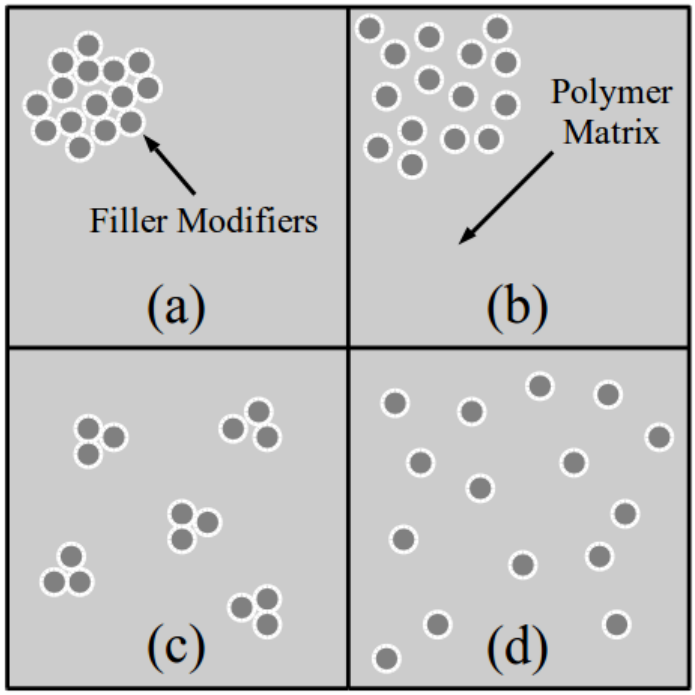

Figure 10 (a) poor dispersion and distribution, (b) good dispersion and poor distribution, (c) good distribution and poor dispersion, (d) good dispersion and distribution

As expected, higher filler concentrations typically lead to higher values of property transfer [39] [95] [85] [102] [103]. However, in addition to processing difficulties due to increasing polymer viscosities, filler volume fractions in multifunctional nanocomposites may be limited by the increasing occurrence of agglomeration zones at higher filler concentrations [39] [102] [98] [99] [100]. Filler addition may also result in the reduction of an inherent polymer property, such as toughness, while adding or enhancing a different property, such as stiffness

[94] [89] [15] [85]. However, both the issues of aggregate-induced macrophase separation and property trade-offs in nanocomposites are a significantly lower risk than in the case of macrocomposites and microcomposites, due to the reduced size of the nanofiller modifiers [77] [37] [80]. Property trade-offs may also be mitigated through the use of multiple filler modifier materials in a single nanocomposite. Thus, for example, organoclay fillers can be used to oppose the lower strength and modulus of rubber-modified polyamide [94] [15] [104] [30].

The three major categories of filler modifiers based on particle shape are particulate, tubular, and layered (platelet-like) materials [94] [87] [105]. Figure 11 shows fibrous and layered materials, by virtue of their shape, possess higher aspect ratios and hence higher surface interaction, whereas particulate fillers provide a lower geometric advantage [94] [86]. Filler enhancement is known to typically be maximized by the smallest nanofillers [83] [91] [40]. Filler materials may be metallic (e. g. aluminium, silver, and copper), ceramic (e. g. boron nitride and silicon carbide), or carbon-based (e. g. carbon nanotubes, graphene, and carbon black) [17] [104] [87] [105].

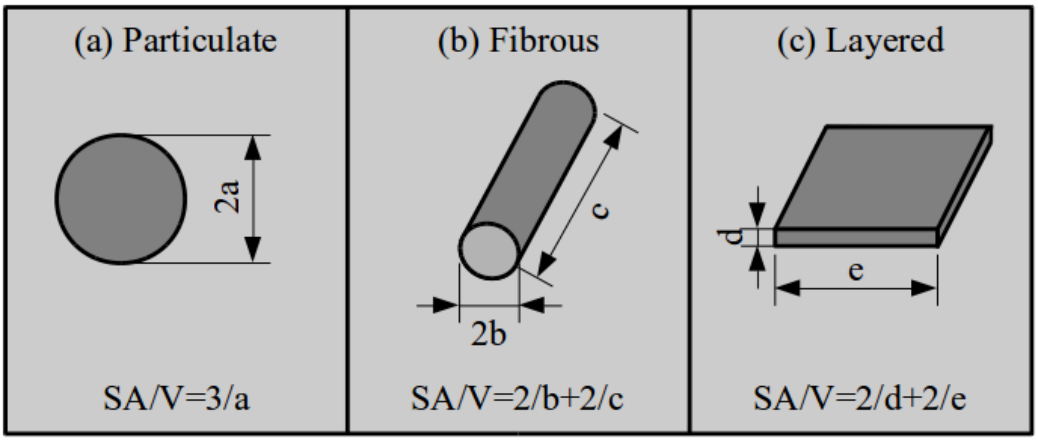

Figure 11 Surface area per unit volume ratios of common (idealized) filler shapes (adapted from *[94]*)

Nanofiller modifiers, like reinforcing fibers for macrocomposites, are used as enhancement materials due to their highly engineered nature, which yields unique and substantially increased properties, e. g. Carbon nanotubes (CNTs) may have Young's Moduli, strengths, and thermal conductivity values as high as 1.4 TPa, 100 GPa, and 6000 W/m-K, respectively [89] [90] [39] [97] [85] [100]. The synthesis of these novel reinforcing nanomaterials may be a gas-phase process (such as plasma heating, laser heating, laser-induced chemical vapor reaction), a liquid-phase process (such as hydrolysis and solvent evaporation), or a solid-phase process (such as thermal decomposition and spark discharge) [38] [77]. By using carbon as a precipitating agent, for instance, in pressured carbonation, nano-scale silica powders may be synthesized for use as multifunctional nanocomposite filler modifiers [38]. These synthesized nanofillers may be further modified to yield additional properties, improve surface adhesion or compatibility between the reinforcing and matrix phases, and to reduce nanoparticle agglomeration and thereby produce a superior nanocomposite [82] [83] [90] [91] [78] [40] [86]. This may involve surface modification, partial chemical modification, external membrane modification, and mechanical and chemical modification [38] [78]. The surface modification of silica nanoparticles, for instance, may be conducted through the use of a chemical coupling agent to reduce agglomeration and increase surface adhesion [91].

In addition to the techniques used for bulk property testing, the nanostructure of nanocomposites is of great interest to research because of the role it plays in property enhancement [38] [97] [93] [37]. Some of the more common techniques in use include Wide Angle X-Ray Diffraction (WAXD), Small Angle X-Ray Scattering, Atomic Force Microscopy, IR Spectroscopy, Scanning Electron Microscopy, and Transmission Electron Microscopy [94] [38] [92] [95] [93] [37]. WAXD may be used to investigate the intercalation or exfoliation of the filler in the nanocomposite by examining the basal reflections of the X-Rays [94] [92] [37]. Transmission electron microscopy provides direct visualisation, using thin films of the nanocomposite material, of the internal structure and spatial distribution of phases [94] [92] [95] [37]. Scanning electron microscopy employs a focused beam of electrons to study surface features on a specimen. This is particularly useful in the examination of fractured surfaces [94] [92] [95].

Unlike macrocomposites, however, the prediction of nanocomposite properties using simple analytical methods, such as the rule of mixtures method, is not always feasible [78] [86] [106] [87]. This is due to the prevalence of complex atomic- and quantum-level phenomena at the phase interface [90] [78] [86] [106] [41]. The percolation threshold, shown in Fig. 12 for instance, in the enhancement of electrical conductivity in nanocomposites, refers to the filler concentration necessary to construct a conductive network in which it is possible for electron tunneling to induce high conductivity due to low distances between highly conductive filler modifiers within the polymer matrix [38] [95] [97] [98] [86] [80]. Many analytical and numerical methods have been proposed for nanocomposite property prediction, but due to the great variation in materials, enhancement properties, and fabrication procedures, as well as the complexities involved in accounting for atomic-scale interactions, there is often disagreement between predicted and experimental values [78] [86] [41] [87].

Although the first nanoclay-polyamide nanocomposite was developed in 1988 by Toyota, their potential for nanocomposite commercialization has not yet been realized [35] [90]. This is due to a number of issues including the high synthesis costs of filler materials, the high costs involved in fabricating superior nanocomposite parts at an industrial scale, and the potential health and safety impact of these materials [35] [90] [98]. Some of the nanocomposite products in use today include batteries, electronic packaging, beverage and food packaging, and tyres [35] [90] [99] [79]. Continuing developments to produce low cost, high efficiency nanofillers and new fabrication processes, as well as new modelling techniques, have helped increase nanocomposite application in recent years [35] [90] [78]. There is also a great deal of interest, as with polymers and polymer macrocomposites, in the development and use of biodegradable and recyclable nanocomposite systems [17] [94] [41].

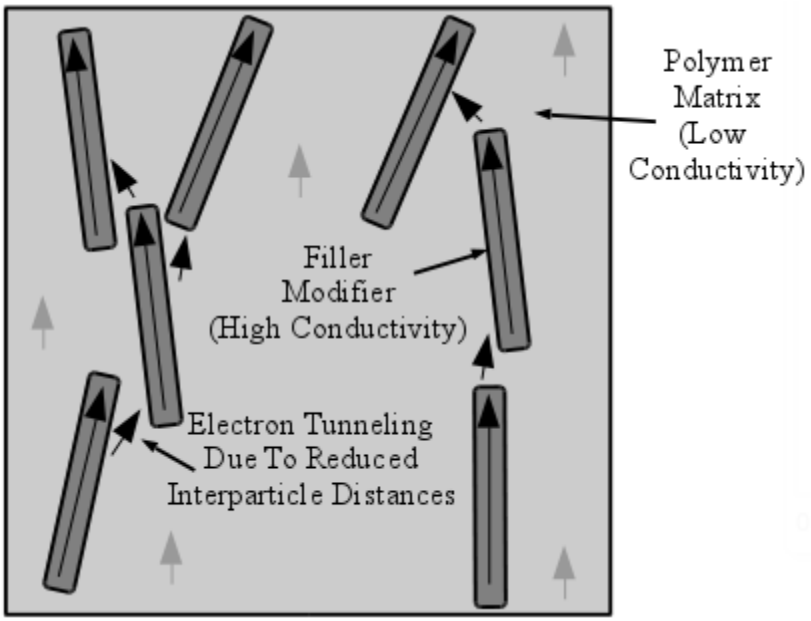

Figure 12 Electrical conduction through percolating network of highly conductive nano-scale filler modifiers

1.5 POLYMER, COMPOSITE, AND NANOCOMPOSITE FABRICATION METHODS

Although there are a number of methods of polymer fabrication in lab and industrial conditions, the curing (or chain extension) process typically involves the use of heat and in some cases, a hardener, to convert a liquid or semisolid prepolymer or quasiprepolymer into a solid polymer part for use [107] [25]. This chain extension causes an increase in viscosity until a solid material is obtained. Further heat causes hydrogen bonds to form, providing additional strength [107]. In order to ensure the most efficient and optimized cure, the material viscosity must be lowered through pre-heating prior to pouring to minimize entrapped air and ensure uniform filling of the mold [107]. Heat must then be applied at a prescribed temperature for a prescribed period of time to complete the curing process [107].

Macrocomposites may be fabricated using a number of continually developing methods, depending on the shape and application of the part as well as the properties of the constituent phases. These can include hand lay-up, filament winding (Fig. 13), vacuum-assisted resin transfer molding, and injection molding [25] [26] [18] [22].

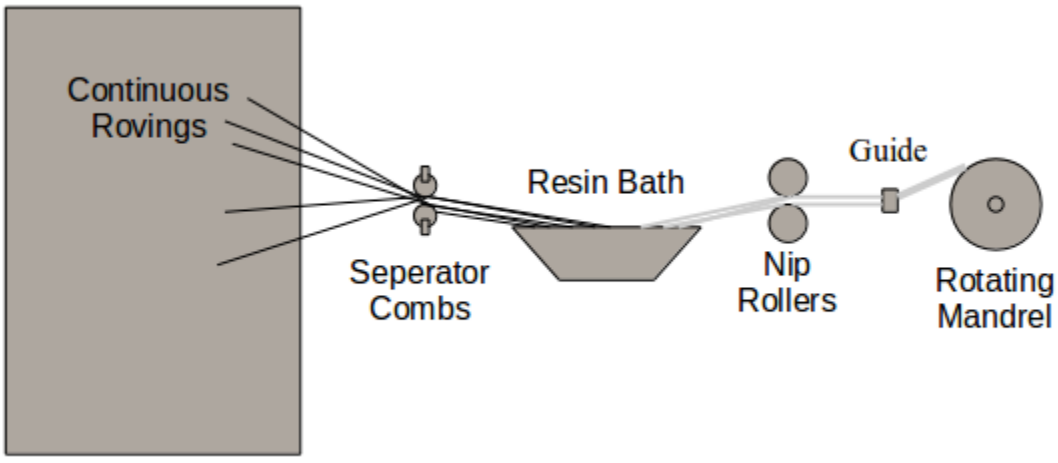

Figure 13 Filament winding procedure (adapted from *[22]*)

In order to achieve a superior part, nanocomposite fabrication typically requires highly exfoliated and distributed nanofillers within the continuous phase [82] [83] [92] [78] [40] [86] [100]. Particle orientation, particularly in the case of fibrous nanofillers, may be manipulated during the fabrication process to provide directional enhancement. Randomly oriented filler modifiers result in isotropic enhancement [82] [39] [84] [95] [98] [86]. In situ methods, such as the sol-gel process, involve the simultaneous synthesis of one or both the reinforcing and continues phase materials [38] [90] [77] [108] [101]. Ex situ methods, in which pre-formed filler modifiers are dispersed in polymers prior to cure include melt mixing, ball milling, and solution blending [82] [108] [97] [98] [93] [101]. The process of solution blending involves the use of a solvent compatible with both the filler and matrix materials to reduce the viscosity of the polymer as well as the agglomeration of the filler material [91] [108] [92] [99] [101]. Upon completion of the mixing stage, which may involve processes such as sonication and automated stirring, the solvent is vaporized prior to polymer curing [94] [38] [83] [91] [92] [37] [101]. Despite the importance of achieving high exfoliation and distribution, care must be taken in fabrication to minimise filler breakage, caused by excessive mixing and sonication, which can result in aspect ratio reduction [105].

1.6 THERMALLY CONDUCTIVE NANOFILLER COMPOSITES

In applications such as electronic packaging, heat exchangers, and thermal pastes, polymer materials offer a great deal of potential, by virtue of their advantages in cost, ease of fabrication, corrosion resistance, and density, but are limited by minimal thermal conductivity values that are typically no more than 0.3 W/m-K at ambient conditions [35] [89] [109] [93] [80] [101] [88] [110] [111] [103] [112]. The inability of polymers in wear and other energy-absorption applications, such as rubber tyres, to efficiently dissipate stored heat can also result in rapid property degradation through oxidation and early failure [67] [79] [80]. To cater to such applications, there has been substantial interest in recent years in the use of highly engineered nano-scale filler modifiers to enhance the thermal transport properties of polymer materials [109] [80] [101] [88] [110] [81] [111] [112].

Although a number of materials (such as metallic or ceramic fillers) may be used to enhance the thermal conductivity of polymer materials, significant research has been invested into the production and application of carbon nanotubes (CNTs) in the development of multifunctional nanocomposites as a result of their superior properties, including high thermal conductivities and aspect ratios [35] [87] [101] [105] [112]. Three weight percent CNT loading, for instance, may be capable of increasing the thermal conductivity of epoxy polymer by 300% [101]. However, due to the high costs associated with their synthesis, as well as the difficulties of minimising structural defects, their application has so far been limited, especially in the enhancement of thermal transport properties [79].

Graphene, which consists of densely packed sp^2-bonded carbon atoms in a single-plane honeycomb lattice, may be wrapped into a tubular shape to produce single-wall CNTs [89] [86] [87] [80] [101] [28] [88]. Graphite nanoplatelets (GNP) are layered or stacked sheets of graphene of varying nano-scale thickness [87] [113] [101] [88]. GNP are considered to be a naturally abundant, lower cost alternative to CNTs for thermal enhancement [87] [80] [101] [88]. As a result of their superior thermal conductivity (ambient in-plane values may be as high as 3000 W/m-K, which are on the same order of magnitude as CNTs), these platelet nanofillers have been successfully utilised, at comparatively low filler loadings, in thermally conductive nanocomposites [100] [113] [80] [28] [88] [110] [103]. By virtue of their geometry, CNTs

possess superior properties in a singular direction whereas GNPs are bi-directionally (or in-plane) conductive [79] [101]. GNPs also offer cost advantages over ceramic fillers and weight advantages over metallic fillers, as well as superior intrinsic conductivity [87] [79] [114]. Furthermore, the use of two-dimensional platelet-like filler modifiers has also been suggested as being more conducive to the enhancement of thermal transport properties as the interface resistance may be reduced by virtue of their geometry [35] [79].

However, the experimental values found (typically under 1 W/m-K enhancement) for thermally enhanced nanocomposites are in the range of those expected from microcomposites (despite the use of nano-scale filler modifiers with high aspect ratios and surface areas). This is significantly lower than the values estimated by models such as the rule of mixtures [87] [110] [115] [116] [103]. Studies have also shown the reduction of neat polymer conductivity upon introduction of highly conductive filler modifiers [87] [80]. This limited or potentially detrimental property transfer has been attributed to the presence of an interfacial thermal resistance between the highly conductive filler modifiers and the polymer matrix [109] [93] [80] [101] [81] [115].

Due to limits on electron motion, quantized vibrational modes within a rigid lattice of molecules, known as phonons, are responsible for heat conduction in polymer materials [87] [79] [103] [112]. A phonon may alternatively be defined as an elementary excitation caused by relative motion of atoms in a lattice [117]. The Debye equation, which relates the specific heat capacity, phonon velocity, and phonon mean free path, may be used to determine the thermal conductivity of polymers [87]. Owing to defect-induced phonon scattering, polymers typically have very small phonon mean free paths of a few angstroms [87] [79]. The length of a phonon mean free path is closely related to the crystallinity of a polymer. Therefore, cross-linked polymers, such as elastomers, have lower thermal conductivities than semi-crystalline thermoplastics [1] [2] [87] [79]. Phonon scattering has also been observed between amorphous and crystal zones in polymers, thus lowering bulk conductivity [87] [79]. Other factors affecting thermal transport properties in polymers include chemical structure, degree of polymerization, structural defects, and processing conditions [87] [79].

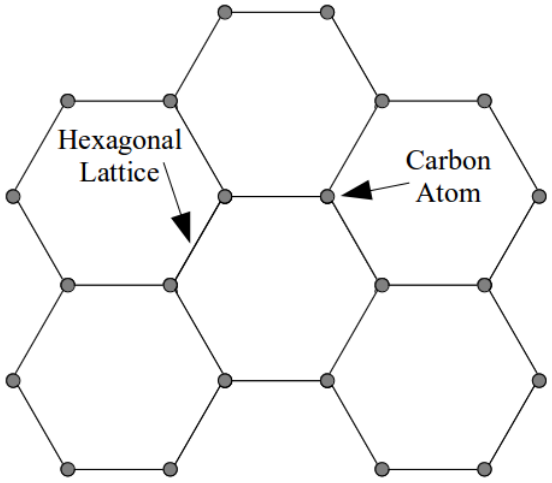

Figure 14 Graphene nanosheet structure (adapted from *[80]*)

By contrast, phonon mean free paths in the highly organized, crystalline, high conductivity nanofillers, tend to be substantially larger, with an estimated value of 500 nm for multi-walled CNTs [87]. This acoustic mismatch (or miscommunication) of vibrational modes due to poor coupling between the highly organized and efficient filler lattice and the disorganized amorphous polymer structure (Fig. 15), resulting in phonon scattering at the phase interface, is known as the Kapitza or interfacial thermal resistance. This is identified as the primary cause of limited thermal property transfer in filler-modified nanocomposites [118] [87] [93] [80] [101] [103] [112]. In addition to phonon mismatch, imperfect contact between the reinforcing and continuous phases, which is highly dependent on surface wettability, also contributes to the interfacial thermal resistance [87] [93] [101] [105]. The Kapitza resistance has been quantified as being on the order of 10^{-8} m^2K/W for CNT-polymer composites [87] [105].

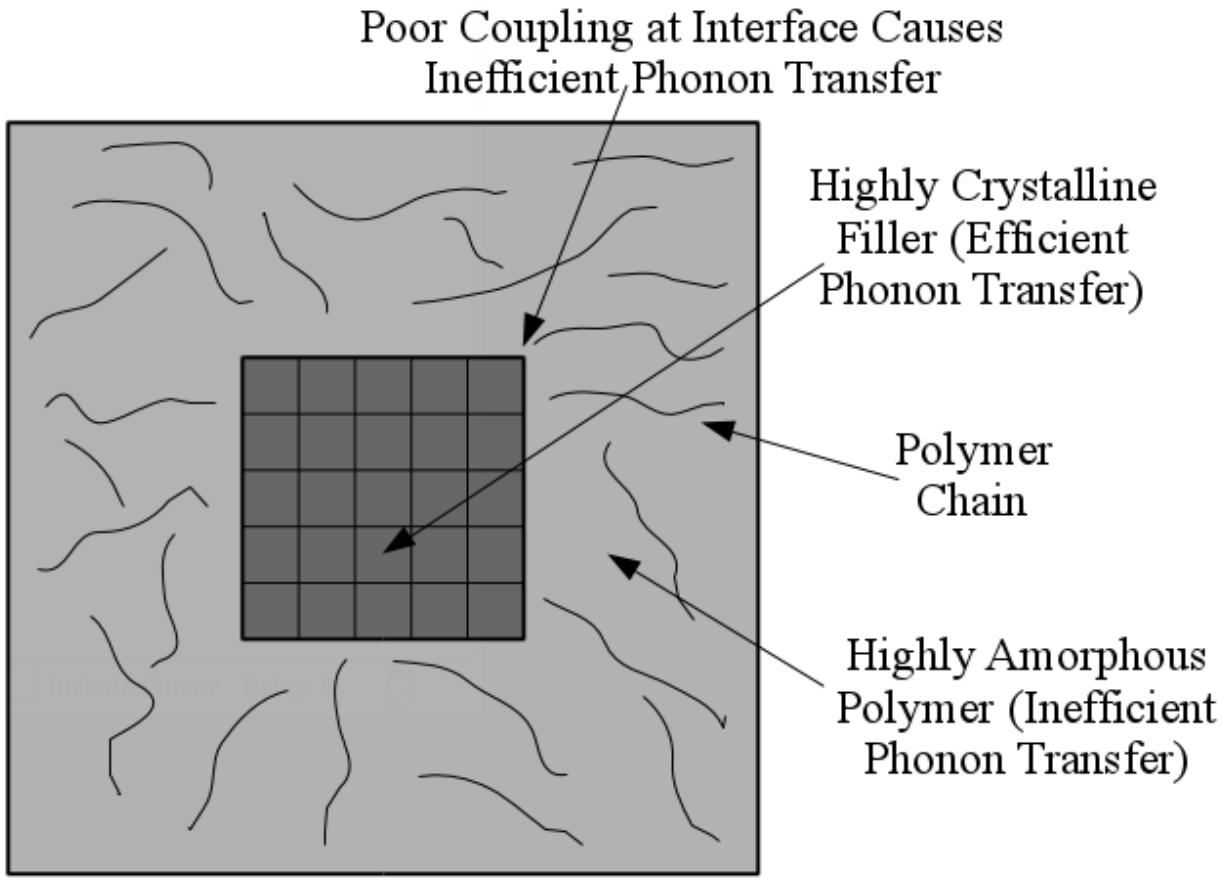

Figure 15 Kapitza resistance caused due to inefficient interfacial phonon transfer resulting from poor phase coupling

Experimental studies have found that the percolating threshold observed in sufficiently loaded electrically enhanced nanocomposites requires substantially higher filler loadings for thermal transport nanocomposites, if at all present [35] [87] [81] [116]. Thermal conductivity enhancement typically follows a linear trend instead [93] [37] [110]. Researchers have proposed that the difference in the thermal and electrical conductivity ratios between phases may be responsible for the inclusion of the matrix phase in thermal transport of nanocomposites, i. e. lack of percolating behavior [87]. The differences in electron and phonon energy transfers mechanisms have also been cited as a potential cause [81]. In the measurement of CNT intrinsic conductivity, results of bundled or agglomerated mats have been found to be multiple orders of magnitude below theoretical estimated values of singular nanotubes due to high thermal contact resistance. However, this contact resistance is significantly lower than the interfacial thermal resistance found in nanocomposites [78] [87] [93] [101] [115] [116] [105].

The primary method of interfacial phonon scatter reduction is to introduce covalent bonding between phases – such filler functionalization may also result in the degradation of intrinsic filler thermal conductivity. This improves the coupling between the filler and matrix particles [87] [105] [103] [112]. Alternatively, controlled filler agglomeration to exploit the comparatively lower contact resistance between filler particles may be a simpler strategy for enhancement. However, there is disagreement on the degree of agglomeration desired due to concerns of uneven distribution, macrophase separation and defects, and increasing agglomerate distances [87] [93] [81]. Likewise, larger filler modifiers within the nano-scale have been shown to increase thermal transport enhancement while reducing the size of particles beyond a critical range begins to yield diminishing returns [109] [105]. Filler alignment, through processing or the use of external force during processing, has also been applied to minimise tube overlap and hence create a directional quasi-percolated conductive network of connected CNT filler modifiers [35] [87] [109] [93] [101] [105]. In addition to the reduction of filler defects, improvement of intrinsic conductivity, and improvement of matrix-reinforcement compatibility, filler functionalization may also be employed to increase molecular attraction between filler modifiers to reduce phonon scatter and hence minimise contact resistance [87] [93] [80] [101] [105] [112]. Synergistic results have been found in the experimental use of multiple or hybrid filler systems, such as CNT/GNP or GNP/Carbon black nanocomposites, due to reduced contact resistance [87] [79] [80] [101].

Due to the complexities of thermal transport and its enhancement discussed above, the property prediction of thermally conductive nanocomposites is challenging [105]. This is further complicated by the large scatter found in experimental results for these nanocomposites [87]. The upper-bound analytical rule of mixtures (parallel) model, which assumes ideal dispersion and percolation substantially overestimates the property of these nanocomposites while the lower-bound series model, which does not assume any network formation, underestimates enhancement [87] [105] [114]. A number of second-order micromechanics models have been proposed, based on the series model, such as Nielsen or Hashin and Shtrikman, have been found to reasonably predict the properties of nanocomposites based on isotropic and low aspect ratio nanofillers [87] [105] [114]. However, these models do not reflect or explain the nature of the micro- and nano-structure of the nanocomposite [87]. Attempts to account for factors such as the

interfacial thermal resistance, anisotropic fillers, and high aspect ratio fillers have also yielded some positive results for selected filler materials [78] [87] [100] [28] [114]. Molecular dynamics simulations may also be performed to find critical variables, such as Kapitza resistance, for use in analytical models [78] [109] [28] [103]. Disagreements continue to appear, however, between predicted and observed values due to the complexities of the nano-scale interactions, variations in materials and fabrication methods, and insufficient nano-structure information [87].

Therefore, in addition to developing superior, lower cost fillers and functionalization methods as well as nanocomposite fabrication techniques for superior thermal transport enhancement, there is also a great deal of focus on the research of developing reliable modelling strategies to accurately understand the mechanics of thermal transport enhancement and hence successfully estimate the thermal conductivity of filler-modified nanocomposite materials [87] [28] [78].

1.7 OBJECTIVES

The objectives of this study were to:

1. Manufacture GNP-modified PU nanocomposite specimens at various filler loadings.
2. Investigate the filler dispersion of the nanocomposite specimens.
3. Experimentally measure the bulk (isotropic) and anisotropic thermal conductivity of the nanocomposite specimens.
4. Using existing analytical models, predict the thermal conductivity of the PU-GNP nanocomposite system and compare to experimental results.
5. Experimentally investigate filler alignment and settling in the nanocomposite.

1.8 THESIS ORGANIZATION

This thesis is organized into a number of chapters. Chapter 2 discusses the experimental work involving the nanocomposite fabrication, analytical models for thermal transport modelling, and experimental test methods to examine the thermal transport enhancement and nanocomposite structure. Chapter 3 includes the descriptions of the second-order analytical models applied in this study for comparison to experimental bulk thermal conductivity results. Chapter 4 discusses the results and analysis of the experimental and analytical work described above. Chapter 5 presents the conclusions of the study and Chapter 6 presents some recommendations for future work based on this thesis study.

2. PROCEDURE

2.1 CURING CHAMBER

Polymer curing typically involves heating the pre-cure material at a prescribed temperature for a prescribed period of time. Fabrication of superior polymer parts also requires that entrapped void zones be minimized. A simple curing chamber apparatus was used to meet these criteria.

The body of the curing chamber, as shown in Fig. 16 and Fig. 17, consisted of a re-purposed 8-inch diameter, 1/4 inch thickness mild steel pipe with a mild steel (1018), 1/4 inch, plate welded to the back. Two holes were made in this back plate – each fitted with a 1/2 inch female NPT (National Pipe Thread) pipe boss. The top pipe was connected via 1/2 inch male pipe connector to a 1/2 inch tube in order to connect the chamber to the vacuum pump. The lower pipe was similarly connected to a modified 1/2 inch male adapter, through which a type T thermocouple, and two copper wires were fed into the body. A mild steel (1018), 3/8 inch, flange was machined flat, fitted with an O-ring groove, and welded to the front of the chamber. A Buna-N O-ring was used in the chamber along with Dow Corning, silicon-based, high vacuum grease (Dow Corning Corporation, Auburn, MI, US) to create a vacuum seal. The front of the chamber, during use, is covered with a 3/4 inch transparent acrylic plate.

Within the chamber body, a 3/4 inch machined flat mild steel (1018) plate was added to house the thermocouple and three 300 Watt OMEGA HDC00101 (OMEGA Engineering, Inc., Norwalk, CT, US) resistance heaters within four drilled cavities. An OMEGA CNi 16D24-C4E (OMEGA Engineering, INC., Norwalk, CT, US) controller was used in conjunction with an OPTEK OSSRD0003A (Optek Technology, INC., Carrollton, TX, US) solid state relay with a maximum output current of 25 amps to control the heaters. To automate the curing process, power was given to these heaters by a GraLab Model 173 15-hour industrial timer (GraLab Corporation, Centerville, OH, US). A 1 inch spherical level was used to balance the plate to ensure uniform thickness in the polymer part. While in use, a pressure of -85 kPa was achieved in the curing chamber using a Precision Scientific Company PS500 double stage vacuum pump.

Figure 16 Curing chamber (external)

Figure 17 Curing chamber (internal)

2.2 SPECIMEN FABRICATION

With a Shore A hardness of 65-70, NR 606 two-part castable urethane PU polymer (Normac Adhesive Products Inc., Burlington, ON, Canada) is primarily used in high wear applications [119]. The PU polymer consists of a Toluene diisocyanate (TDI) isocyanate and a polyether polyol [119]. Prior to fabrication, NR 606 part A was pre-heated to 30°C in order to improve processability. Using M209-4 methyl ethyl ketone (MEK) solvent (Fisher Scientific Company, Ottawa, ON, Canada), PU viscosity was reduced to allow solution blending of Grade M 5-micron bulk dry powder GNP nanofillers (XG Sciences, Inc., Lansing, MI, USA) [119] [113]. Both neat and GNP-modified PU were fabricated using the following method.

Frekote 700 NC release agent (Henkel Corporation, Düsseldorf, Germany) was added to a 1/2 inch base, 1/4 inch side, open-style, machined flat, disassesambleable mild steel (1018) mold to allow easy post-cure removal of the part. A prescribed mass of GNP nanoparticles was added to MEK solvent and stirred manually. NR 606 part A prepolymer was then added to the solution and mixed manually, prior to ultrasonication using a Q500 sonicator (Qsonica, Newtown, CT, USA) set to a power, amplitude, and frequency of 500 Watts, 100%, and 1 Hz, respectively, for one hour, to disintegrate graphite aggregates in the bulk dry powder and thus reduce filler aggregation. The solution was then magnetically stirred at a temperature of 35°C for one hour to encourage high filler distribution in the polymer. Using a vacuum pump, the MEK solvent was vaporized at a pressure of -85 kPa prior to addition of NR 606 part B. The mixture was carefully de-gassed beyond the point of foaming, which is known to occur in PU due to absorbed moisture, to minimize void zones [107]. Finally, the solution was transferred to the curing chamber, in the open mold, and heated at 80°C and a pressure of -85 kPa for four hours.

PU was retrieved from the mold post-cure and nine square specimens of approximately 35 mm side were removed from the plaques using a Delta 52-965, 14 inch, 4 teeth per inch band saw (Delta Power Equipment Corp., Anderson County, SC, US). The specimens were finally cleaned with A18-4 acetone to prepare for testing (Fisher Scientific Company, Ottawa, ON, Canada).

2.3 X-RAY DIFFRACTION

The primary benefit of scattering methods, such as X-Ray Diffraction (XRD), over microscopy techniques is the ability to perform bulk analysis on test specimens [120]. However, while scattering techniques produce results only in reciprocal space, microscopy results are taken in real space [120]. In XRD analysis, when X-Rays make contact with a test specimen, electrons within become excited, causing periodic vibrations, and thus electromagnetic waves of a particular frequency and wavelength [120]. The original X-Rays are scattered by these waves and the resulting scatter yields information about the test specimen [120]. Amorphous materials, for instance, provide diffused patterns, whereas crystalline materials cause sharp diffraction peaks to appear [120]. The Bragg Law, Equation 1 below, defines the relationship between the wavelength of the original beam, the diffraction intensity and angle, and the d-spacing between crystal lattice planes [120].

$$n\lambda = 2d_{hkl}\sin\theta \tag{1}$$

Wide-angle X-Ray Diffraction (WAXD) may be used to analyze features smaller than 30-40 Angstroms (3-4 nanometers), as diffraction peaks occurring at angles larger than 2° are detected through this technique [120]. Thus, it is possible to analyze the nanostructure of a polymer nanocomposite using WAXD [120]. In the fabrication of multifunctional nanocomposite materials, filler aggregation is typically discouraged with the aim of achieving perfect exfoliation in order to increase the interfacial surface area and hence, property enhancement [120]. Highly dispersed or exfoliated filler modifiers in a nanocomposite system may result in the disappearance of diffraction peaks – however, TEM analysis has shown aggregate presence in certain cases despite the disappearance of basal peak [120]. Although peak width and intensity can be influenced by filler dispersion and orientation, this does not serve as a reliable metric for such characterization due to the fact that width and intensity may also be altered by factors such as interference effects, polarization, and issues in fabrication [120]. The shift of basal (symmetrical) peaks towards smaller angles, in the case of materials such as layered silica filler modifiers, is considered to be a stronger indication of superior dispersion and exfoliation [120]. In such cases, an increase in d-spacing comparable to the height of a polymer chain proves matrix intercalation within silica layers [120].

WAXD was performed on the mold side of test specimens on a Rigaku Ultima IV Multipurpose X-ray diffraction system (Rigaku Corporation, Tokyo, Japan) using a Cobalt tube and a wavelength of 1.78899Å under a voltage of 38 kV and a current of 38 mA. Two test specimens were selected from each specimen set for XRD characterization.

2.4 TRANSIENT PLANE SOURCE THERMAL CHARACTERIZATION

The Thermtest Transient Plane Source (TPS) 2500S Hot Disk thermal constants analyzer (TCA) (Thermtest Inc., Fredericton, NB, Canada) was used to determine the thermal conductivity of the PU specimens with the CS5501 sensor at 21°C.

The Hot Disk analyzer utilizes the TPS method, described in ISO 22007-2 to determine the thermal transport properties of a given specimen, with the aid of a disk-shaped, double spiral sensor [121] [115]. As opposed to the hot strip and wire sensors, by virtue of its geometry, the hot disk sensor possesses higher initial resistance and also allows the use of smaller specimens [121]. Transient measurement techniques such as the laser flash or step method may only be used to determine the thermal diffusivity of a specimen and not its thermal conductivity, since the heat applied to the specimen cannot be determined, while the TPS hot disk method may be used to find both [121] [115] [105]. The TPS method also offers advantages over steady state thermal transport analysis methods, such as the guarded hot plate technique, in specimen size and preparation [121]. The hot disk sensor serves the dual role of heater and resistance thermometer – through the introduction of an electrical current, the sensor's temperature is increased while simultaneously recording its change in resistance as a function of time [121] [115] [105]. Typically consisting of 10 μm spirally-wound Nickel-metal, the sensor is encased in a protective layer of polyimide film to ensure electrical insulation [121] [115] [105].

The sensor is placed between two test specimens and heated at a prescribed setting (heating rate) for a prescribed duration (measurement time) as 200 resistance readings are taken to develop a time-temperature relationship [121] [115] [105]. The basic inputs available through the hot disk sensor include the heat added to the specimens and the resistance of the sensor [122] [121]. The principal of the hot disk method involves, under the application of this sensor heat to a theoretically infinite specimen (i. e. no detection of external media), finding the time-dependent increase in average temperature at the sensor surface [122] [121]. The increase in temperature at the sensor surface allows the calculation of specimen thermal diffusivity and thermal conductivity [121] [122]. In order to ensure that the bounds of the test media are not violated, the measurement time is carefully calibrated [122] [121] [115].

The basic heat conduction is solved for three dimensions and time including a heat source consisting of multiple equidistant concentric ring heat sources to relate the known heat flux added by the sensor to the time-dependent average temperature increase for the sensor surface [121] [122]. This results in the following expression.

$$\Delta T_{AVG}(\tau) = \frac{PD(\tau)}{r_s k \pi^{\frac{3}{2}}} \tag{2}$$

$$\tau = \sqrt{\frac{t}{\Theta}} \tag{3}$$

$$\Theta = \frac{r^2}{\alpha} \tag{4}$$

The resistance of the sensor is used to find the time-dependent temperature increase through the following resistance-temperature relation [122] [121].

$$R(t) = R_0(1 + \mathrm{A}(\Delta T_i + \Delta T_{AVG}(\tau))) \tag{5}$$

Through algebraic manipulation, the temperature change recorded may be determined as shown below [122] [121].

$$\Delta T_{AVG}(\tau) + \Delta T_i = \frac{1}{\mathrm{A}}\left(\frac{R(t)}{R_0} - 1\right) \tag{6}$$

ΔT_i, the thermal contact or temperature difference between the sensor and the specimen surface becomes constant after a very short period of time, which depends on the properties of the insulating polyamide layers and may be defined as [122] [121]:

$$\Delta t_i = \frac{\xi^2}{\alpha_i} \tag{7}$$

A linear computational plot of the $D(\tau)$ function against the recorded temperature change will be found to have an intercept at ΔT_i and a slope of $P/kr\pi^{3/2}$, under experimental conditions in which the measurement time is significantly longer than Δt_i [122] [121] [105]. The calculation

involved in the plotting of the final straight line used here is an iterative process, due to the fact that the thermal diffusivity is not known prior to experimentation [121] [122].

The apparatus may also be used to determine the thermal transport properties of anisotropic materials possessing differing properties in the in-plane and through-thickness directions [121]. With known values of X ($\sqrt{(k_a k_r)}$), Y (α_a), and Z (ρC_p), the following relations are used to determine the directional conductivities and diffusivities. While the test apparatus provides values X and Y, Z must be independently determined [123]:

$$\Delta T_{AVG}(\tau) = \frac{PD(\tau)}{rX\pi^{\frac{3}{2}}} \tag{8}$$

$$\tau = \sqrt{\frac{t}{\Theta_a}} \tag{9}$$

$$\Theta = \frac{r^2}{\alpha_a} \tag{10}$$

Therefore, using the following equations, the final directional properties can be determined for the specimens [123]:

$$\alpha_a = Y \tag{11}$$

$$k_a = Z\alpha_a \tag{12}$$

$$k_r = \frac{X^2}{k_a} = \frac{X^2}{\rho C_p Y} \tag{13}$$

$$\alpha_r = \frac{k_r}{\rho C_p} = \frac{X^2}{Y(\rho C_p)^2} \tag{14}$$

After measuring their smallest dimension (thickness), specimens with similar values were paired for testing. Two-sided bulk and anisotropic testing were performed using four specimen sets from each filler-modified weight group, as shown in Fig. 18 below. Two readings were taken for each set adjusting the heating power and measurement time in each case to ensure

maximum penetration depth of the specimens without exceeding the material boundaries. The drift period was set to 40 seconds for all tests. A fifteen minute wait period between tests allowed the specimens to cool to prevent test-induced temperature increases to influence results. Data found not to fall within the recommended mean deviation parameter of 10^{-3} or lower were rejected as higher values are considered indicative of errors [115]. Obtained values were then averaged to produce thermal conductivity values for each specimen group.

In order to test the specimens for settling effects, anisotropic testing was performed on the single largest specimen pair from each filler weight group at varying heating rates and test durations to penetrate to prescribed sections (axial probing depth) of the test specimens. In some cases, data points were removed from the latter sections of the recorded data until the prescribed probing depth was achieved. These thermal conductivity values were then compared to investigate settling and alignment of filler modifiers in the PU nanocomposites.

Figure 18 Thermtest sensor prior to and during testing sandwiched between test specimens fixed in test rig

2.5 DIFFERENTIAL SCANNING CALORIMETRY

The directional (in-plane vs through-thickness) thermal conductivity of a test specimen may be found using the Thermtest TPS 2500 S TCA given the volumetric heat capacity of the specimen [123]. Dimensional measurements were taken of a number of four specimens (at various points to minimize effects of varying height) from each group, along with their mass, to find the densities of the specimens.

In accordance with ASTM standard E1269, DSC testing was performed to find the specific heat capacity of the specimens per unit mass using a Mettler Toledo DSC 2 Instrument with 40 μL Mettler Toledo standard Aluminum crucibles (Mettler-Toledo, LLC , Columbus, OH, US) [124]. The test was run on an empty pan (baseline), a sapphire standard (used due to its well-documented specific heat capacity over a wide range of temperatures), and the specimen itself. Specimens used were of similar mass to the sapphire standard.

Under the E1269 test method, the baseline run is used to remove the effects of the crucible from the sapphire and test specimen results. The heat flow offset between these runs is then compared to determine the specific heat capacity per unit mass of the test specimen.

In order to find the optimal heating rate, multiple runs were performed until the standard 20°C/min test rate was selected. Testing was performed under a three-segment program consisting of isothermal (0 °C), dynamic (0 to 40 °C), and isothermal (40 °C) with the isothermal segments lasting five minutes each time. Weighing the pans after each test indicated that no mass loss occurred during testing. Two tests were performed on each specimen and an average of the results was taken.

The volumetric specific heat capacity values for each specimen set were then found using the average specific heat capacities and the average densities.

2.6 COMPRESSION TESTING

In order to assess the state of filler alignment within the test specimens, compression testing was performed on each of the principle axes, for small cube-like specimens. These specimens were cut with a razor blade. Compression testing was performed on an MTS Synergie/Bionix 400 frame (MTS Systems Corporation, Eden Prairie, MN, USA) equipped with 500 N load cell using custom-made mild steel (1018) compression plattens, as shown in Fig. 19 below. With a maximum load limit of 350 N and a maximum displacement limit of 2.5 mm, data was acquired at a rate of 10 Hz with a test speed of 5 mm/min (with a pre-load 0.1 N displacement of 40 mm/min) in a displacement control test.

Three specimens were tested from each specimen set in each of the three directions such that the first specimen was tested in the thickness or A-direction, then in the width or B-direction, and finally in the length or C-direction as indicated by Fig. 20 below. The procedure was then repeated in a BCA order for the second specimen and a CAB order for the third and final specimen in the set. This was done to eliminate the effect of plastic deformation during the first test for comparison. The linear sections of the stress-strain curves were than examined to find the compressive modulus values for the specimens. Filler alignment was investigated by comparing the modulus values of directions B and C (radial or in-plane) to direction A (axial or through-thickness) within test sets.

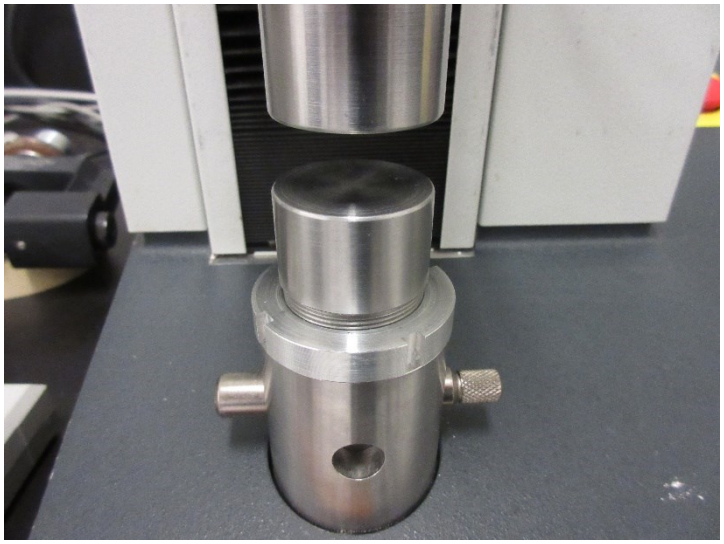

Figure 19 MTS Synergie/Bionix 400 frame with custom compression plattens

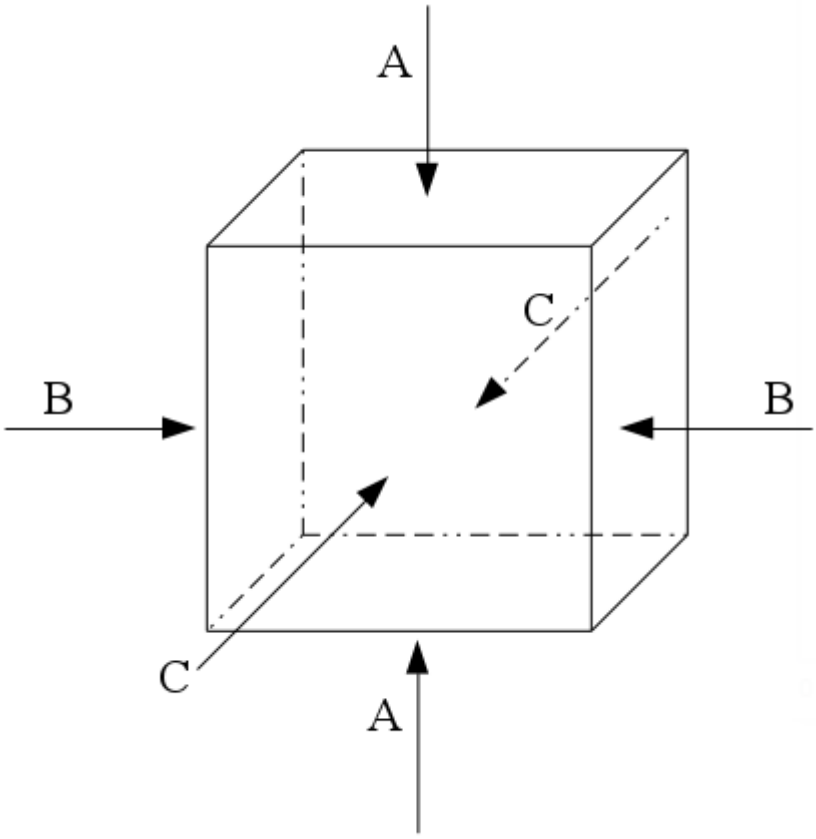

Figure 20 Cube-like ompression specimen under testing in directions A, B, and C, for modulus comparison

3. ANALYTICAL MODELLING

As discussed in section 1.6, there have been several attempts to model the thermal conductivity of two-phase nanocomposite systems. Some of these analytical models were applied to the PU-GNP nanocomposite and compared to the experimental results for thermal conductivity.

The simplest approaches for two-phase thermal conductivity modelling, the upper-bound (parallel, rule of mixtures) and lower-bound (series) models may be derived by comparison to electrical conductivity as follows [125]. The thermal resistance to heat flow at steady state may be defined under equations 15 and 16 for thermal measurement and material property and dimensions, respectively [125].

$$R = \frac{\Delta T}{Q} \tag{15}$$

$$R = \frac{x}{k} \tag{16}$$

Through the use of Fig. 21 below, the total thermal resistance of the one-dimensional multi-phase material can be defined using equations 17 and 18 below, for the series model (a), as the thermal resistance is additive and using equation 19, for the parallel model (b), as the inverse thermal resistance is additive [125].

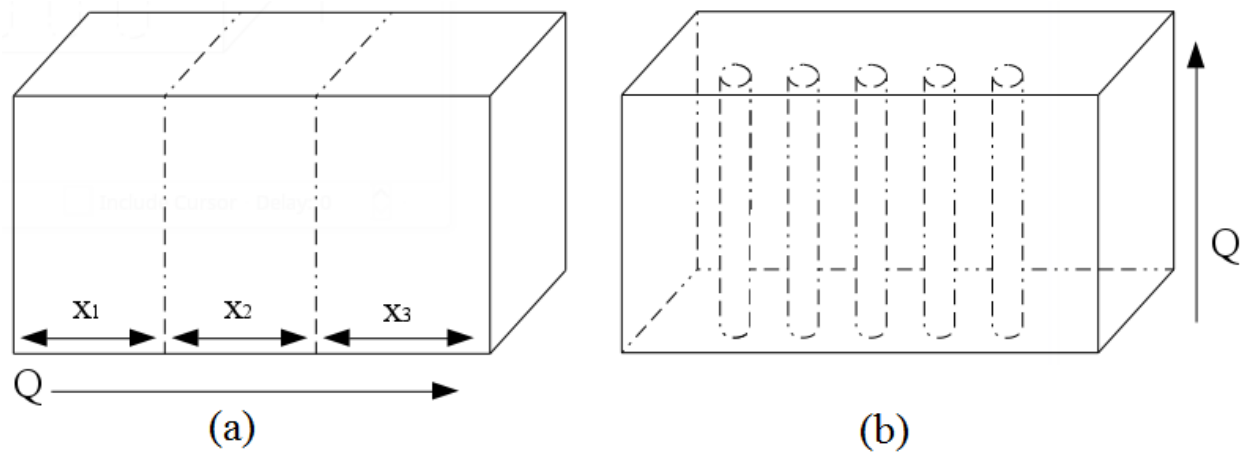

Figure 21 (a) Series model and (b) Parallel model for thermal conductivity (adapted from *[125]*)

$$R = \frac{\sum \Delta T_n}{Q} = \sum R_n = \sum \frac{x_n}{k_n} = \frac{x}{k} \tag{17}$$

$$\frac{1}{k} = \sum \frac{1}{k_n}\left(\frac{x_n}{x}\right) \tag{18}$$

$$k = \sum \frac{x_n}{x} k_n \tag{19}$$

While the parallel model assumes a perfect network of filler modifiers contributing to property transfer depending on the filler volume fraction (FVF), the series model considers each particle to be operating independently of all others (i.e. non-interacting dispersed phase) [87] [125]. Experimental results are typically found to fall within the upper- and lower-bound models, Equations 20 and 21 below simplified for application to two-phase systems, in much closer agreement to the lower-bound model [87] [125].

$$k_{\mathrm{nc}} = k_{\mathrm{f}} FVF + k_{\mathrm{m}}(1 - FVF) \tag{20}$$

$$k_{\mathrm{nc}} = \frac{1}{(1 - FVF)/k_{\mathrm{m}} + FVF/k_{\mathrm{f}}} \tag{21}$$

Based on the lower-bound series model, a number of second-order models, such as the Maxwell model, were developed [125]. Maxwell's approach, based on interfacial potential and electrical continuity, resulted in Equation 22 [126] [125]. The model describes the effective specific resistance of a two-phase material consisting of a low conductivity continuum into which are dispersed high conductivity non-interacting spheres [125]. The Maxwell model performs best for highly dispersed spherical filler particles at low filler volumes with no interfacial resistance [125].

$$k_{\mathrm{nc}} = k_{\mathrm{m}}\left[\frac{2k_{\mathrm{m}} + k_{\mathrm{f}} + 2FVF(k_{\mathrm{f}} - k_{\mathrm{m}})}{2k_{\mathrm{m}} + k_{\mathrm{f}} - FVF(k_{\mathrm{f}} - k_{\mathrm{m}})}\right] \tag{22}$$

The Bruggeman model, developed from the Maxwell model, is reduced to Equation 23 under the assumption of negligible interfacial thermal (Kapitza) resistance between the nanocomposite filler and matrix phases [126] [125]. Through Bruggeman's embedding

integration methodology, this model accounts for some level of particle interaction [125]. Although the Bruggeman model performs well at higher filler loadings, it also predicts percolation at 33% volume fraction, which has not been observed in practice [127] [126] [125].

$$1 - FVF = \left[\frac{k_f - k_{nc}}{k_f - k_m} \right] \left(\frac{k_m}{k_{nc}} \right)^{1/3} \tag{23}$$

Based on the Halpin-Tsai micromechanics equations, the Nielsen model, as shown in Equations 24-26 below, was developed to predict thermal conductivity in nanocomposites [126] [87] [127] [125] [128]. In this case, the conductivity may be compared to stiffness or elastic shear modulus and the flux disturbance may be compared to the stress field disturbance [125]. The Nielsen model introduces the shape factor *M*, based on the generalized Einstein coefficient determined by the filler shape and orientation in relation to the direction of heat flux, and the maximum packing fraction, determined by the filler shape and arrangement [126] [87] [127] [125] [128]. The introduction of maximum packing fraction provides a reduced filler loading value, thus amplifying the effect of increased filler inclusion at higher volume fractions [127] [87] [125]. This means that the highest possible filler loading is no longer 100%. Allowing for full filler loading is an unrealistic assumption since this condition cannot he realized in reality [125]. Hence, the Nielsen model has superior performance at higher loading [87] [125]. However, the model does not account for interfacial resistance [125].

$$k_{nc} = k_m \left[\frac{1 + M * L * FVF}{1 - \varphi * L * FVF} \right] \tag{24}$$

$$\varphi = 1 + \frac{(1 - FVF_{MAX})FVF}{FVF_{MAX}^{\ 2}} \tag{25}$$

$$L = \frac{k_f / k_m - 1}{k_f / k_m + M} \tag{26}$$

The equivalent inclusion method for micromechanics was adapted for heat conduction by Hatta and Taya [125]. This method involves the replacement of a filler of conductivity k_f with an inclusion of conductivity k_m with a volume distribution of dipoles allowing the same thermal intensity field as the particle for the equivalent inclusion [125]. The Hatta and Taya method can

account for some level of filler interaction [125]. It may also be applied, as shown below in Equations 27-29, in contrast to the above, to disc or platelet-like particles due to the dimensionless shape factor N [127] [125].

$$k_{\mathrm{nc}} = k_{\mathrm{m}} + \frac{k_{\mathrm{m}} FVF}{N(1-FVF) + k_{\mathrm{m}} / (k_{\mathrm{f}} - k_{\mathrm{m}})} \tag{27}$$

$$N_{\text{IN-PLANE}} = \pi r / 2s \tag{28}$$

$$N_{\text{THICKNESS}} = 1 - \pi r / s \tag{29}$$

4. RESULTS AND DISCUSSION

4.1 MATERIAL CHARACTERISATION

Using the curing chamber, ten usable polymer nanocomposite plaques were fabricated from a range of 0% to 4% filler weight content. Due to the difficulties found in material processing and fabrication, particularly in mixing and pouring, due to the highly viscous nature of the PU polymer, 4% was the highest filler weight content plaque successfully fabricated [119]. Plaques found to have visible air pockets or other unusual characteristics in either plaque surface were rejected. Plaques were also rejected if found to have visible air voids when cut for testing or highly uneven thickness across the plaque. However, some void presence is still to be expected in the plaques.

Each of the ten plaques was cut into nine specimens thus producing specimen sets containing 0%, 1%, 2%, 3%, and 4% filler modifiers. The specimen cut from the center of the plaque in each case was selected for XRD and compression testing while the thickest remaining specimens were selected for Thermtest analysis. Some of the other specimens were used for DSC analysis.

XRD analysis of filler-modified specimens showed four major peaks at 23.3°, 31°, 52°, and 64.4°. These were identified, through results of XRD analysis on neat PU polymer and graphite powder, to be induced by polyurethane, graphite, polyurethane, and graphite, respectively. WAXD plots are included in the appendix.

The second sharp diffraction peak was identified as the symmetrical crystalline graphite peak and used to find the d-spacing between neighboring nanoplatelets. Although the height of the peak varied among the tests, comparisons between the dry powder and various modified nanocomposite specimens showed a uniform d-spacing of 3.35 angstroms thus confirming that despite the use of ultrasonication, intercalation had not occurred in the nanocomposite and that the filler modifier had aggregated into tactoids throughout the specimen, i. e. poor filler dispersion. The fillers may be considered to be phase-separated agglomerates in the continuous phase. Additionally, since the filler weight introduced to the nanocomposite was measured as bulk dry powder, the density of the filler modifier within the nanocomposite may be taken as that

of the bulk dry powder, as opposed to the density of the nanoplatelet, given by the supplier as 30-100 kg/m^3, for calculation [113].

4.2 ISOTROPIC ANALYSIS

Taking the polyurethane matrix density, provided by the supplier as 1040 kg/m^3, and arbitrarily selecting a filler density of 65 kg/m^3 based on the data discussed in section 4.1, the filler volume fraction was found using Equation 37, as derived from Equation 30, below [119] [113]. However, it must be noted that due to the presence of entrapped air voids, as discussed in section 4.1 above, the theoretical filler volume fraction found using Equation 37 will not be fully representative of the experimental specimens.

Equations 20-29 were then applied to the nanocomposite material to determine its thermal conductivity according to each of the analytical models and compared with the experimental results, as shown in Table 1 and Fig. 22 below. With the exception of the Hatta and Taya model, the filler modifiers were assumed to be isotropic randomly dispersed spherical fillers, due to the limitations of the models [87] [127] [126] [125] [128]. The graphite nanoplatelets' thermal conductivity was taken as 3000 W/m-K while the average radius and thickness were taken as 2.5 μm and 7 nm as provided by the supplier [113]. PU conductivity, typically given as 0.2 W/m-K, was also found experimentally in the neat polymer specimens and therefore used for calculation [71]. In the application of the Nielsen model, the shape factor *M* and the maximum packing fraction (or maximum filler volume fraction) are taken as 1.5 and 63.7% respectively [125] [128].

$$FVF = \frac{V_f}{V_f + V_m} \tag{30}$$

$$FVF\left[\frac{V_f + V_m}{V_f}\right] = 1 \tag{31}$$

$$FVF\left[\frac{V_m}{V_f} + 1\right] = 1 \tag{32}$$

$$FVF\left[\left(\frac{V_m}{V_f}\right)\left(\frac{\rho_m}{\rho_f}\right)\left(\frac{\rho_f}{\rho_m}\right) + 1\right] = 1 \tag{33}$$

$$FVF\left[\left(\frac{V_m\rho_m + V_f\rho_f - V_f\rho_f}{V_f\rho_f}\right)\left(\frac{\rho_f}{\rho_m}\right)+1\right]=1 \tag{34}$$

$$FVF\left[\left(\frac{W_m + W_f}{W_f}-1\right)\left(\frac{\rho_f}{\rho_m}\right)+1\right]=1 \tag{35}$$

$$FVF\left[\left(\frac{1}{FWF}-1\right)\left(\frac{\rho_f}{\rho_m}\right)+1\right]=1 \tag{36}$$

$$FVF=\frac{1}{\left[1+\left(\frac{\rho_f}{\rho_m}\right)\left(\frac{1}{FWF}-1\right)\right]} \tag{37}$$

Table 1 Theoretical and experimental data at various filler loadings for PU-GNP nanocomposite

Filler weight fraction (%vol)	Filler volume fraction (%wt)	Experimental (W/m-K)	Rule of mixtures (W/m-K)	Lower-bound (W/m-K)	Maxwell (W/m-K)	Bruggeman (W/m-K)	Nielsen (W/m-K)	Hatta and Taya (In-plane) (W/m-K)	Hatta and Taya (Thickness) (W/m-K)
0%	0%	0.20	0.20	0.20	0.20	0.20	0.20	0.20	0.20
1%	14%	0.26	417.56	0.23	0.30	0.31	0.29	0.20	0.20
2%	25%	0.31	738.61	0.27	0.40	0.47	0.39	0.20	0.20
3%	33%	0.36	993.24	0.30	0.50	0.67	0.52	0.20	0.20
4%	40%	0.43	1200.1	0.33	0.60	0.92	0.70	0.20	0.20

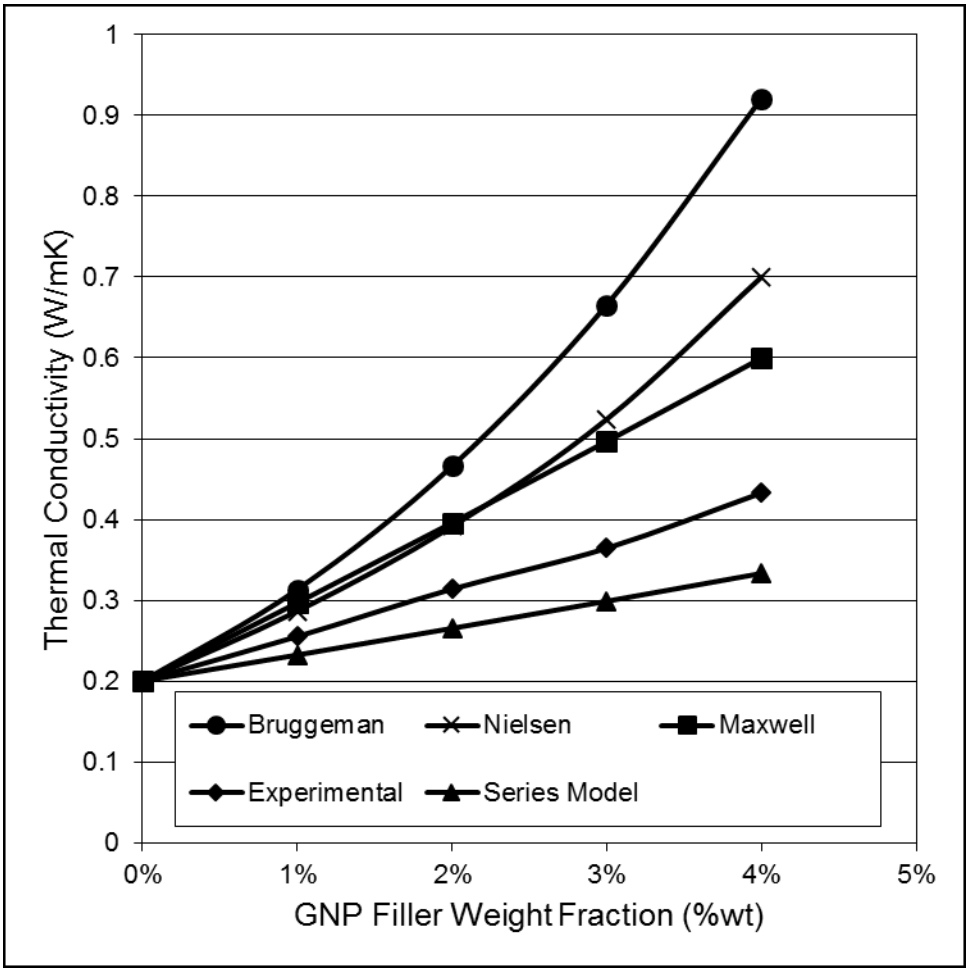

Figure 22 Theoretical (selected) and experimental data for PU-GNP nanocomposite at various filler loadings

While Table 1 includes all experimental and theoretical data, results found for the rule of mixtures and Hatta and Taya models were too high and too low respectively to be compared to the experimental values in Fig. 22. This is expected, in the case of the rule of mixtures, as it is known to highly overestimate the nanocomposite thermal conductivity [87]. The Hatta and Taya model likely breaks down as a result of the extreme aspect ratio of 700 (using the values assumed above) [113].

As expected from literature, the lower-bound series model falls slightly below the experimental results, while mostly observing a similar linear trend, with the disagreement increasing as filler loading is increased [87] [125]. By comparison, each of the remaining models, while again adhering to a similar trend, show a greater disparity with the experimental

values observed, becoming further diverged with increasing filler loading. Bruggeman's model, developed from the Maxwell model, provides the highest set of values among the set [126] [125]. This is expected as the Bruggeman model predicts percolation to occur at 33% filler volume fraction, which may be verified by the rapid change in slope between 3% and 4% filler weight fraction [127]. The disparity between the experimental values and the Bruggeman result may also be due to the assumption of negligible interfacial resistance between the phases [125].

As the selected filler density value of 65 kg/m^3 was arbitrarily chosen, a number of alternative filler densities were also examined for modelling purposes. The maximum bulk powder density provided by the supplier, of 100 kg/m^3, illustrated in Fig. 23 below, was of particular interest as it results in a high agreement between the Nielsen and Maxwell models and the experimental thermal conductivity values of the nanocomposite [113]. This may be due to the fact that the phase-separated agglomerates can be considered comparable to the spherical inclusions assumed under the Maxwell and Nielsen models here. However, there is some disagreement between the experimental and theoretical results at the latter points due to the fact that the models overestimate filler enhancement effect after 30% filler volume. Overall, this suggests that the Nielsen and Maxwell models may be used, under the assumed density value of 100 kg/m^3, to predict the behavior of this nanocomposite system. In the examination of the nanoplatelet density of 2,200 kg/m^3, modelling results were found to be universally lower than the experimental values [113]. Despite the fact that these second-order models are often, as in this case, found to mostly agree with experimental results, it must be noted that they are not reflective of the internal structure of the polymer nanocomposite [87] [105] [114].

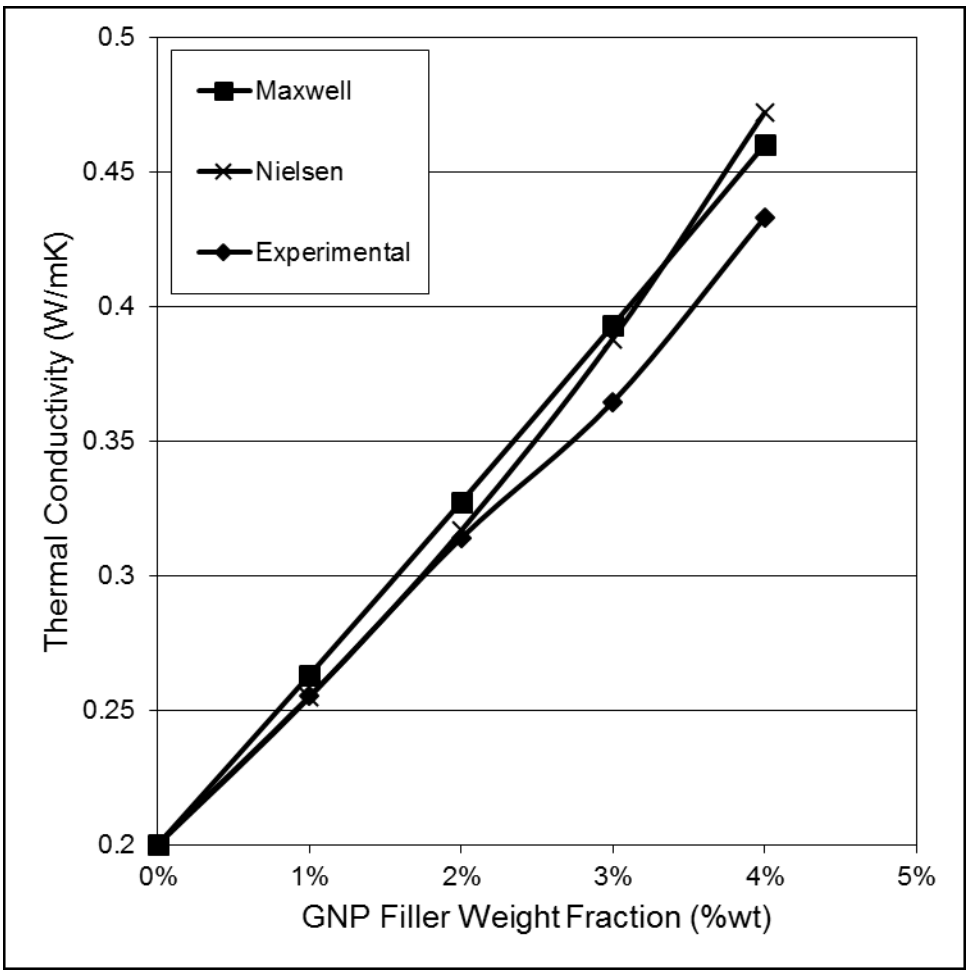

Figure 23 Theoretical (selected) and experimental data for PU-GNP nanocomposite at various filler loadings under 100 kg/m3 assumed filler density

As discussed above, the majority of the models applied in this study assume spherical isotropic fillers, while in reality the filler modifiers in this case are highly anisotropic platelet or disc-like flakes. These analytical models also assume a fully two-phase system without any air voids present [127]. Through the use of the curing chamber and careful fabrication and quality control methods, void content was minimised in this study; however, it is unlikely to have been fully eliminated. This is because the PU polymer is highly viscous even at high temperatures and requires a substantial vacuum pressure as well as time to be thoroughly degassed. Since the curing process must be induced shortly after the introduction of part B, this results in a limited time window for degassing. For these reasons, voids are expected to have been present, albeit in a limited quantity, in the test specimens. Despite the thorough vaporization procedure involved

in removing the MEK solvent prior to cure, trace amount of solvent or additional impurity present in the final test specimen further removes the experimental conditions from an idealized analytical model.

As discussed in section 4.1, processing difficulties limited the filler content in the nanocomposite to 4% weight (or 40% volume assuming filler density of 65 kg/m^3). As seen in other studies, despite this high filler content, percolation behavior does not appear at any point for this nanocomposite material system [35] [87] [81] [116]. A practically linear curve was instead observed which is typical for nanocomposites enhanced for thermal conductivity [93] [37] [110]. With an intercept value of 0.2 W/m-K (experimental value found for the thermal conductivity of neat PU polymer), the linear best-fit slope for the filler weight fraction thermal conductivity curve was 5.7 W/m-K. Considering the high intrinsic conductivity of the graphite nanoplatelets filler modifiers, this is a very low enhancement effect. Using the lower through-thickness conductivity of 6 W/m-K for the material, the rule of mixtures value at the 40% filler volume fraction for nanocomposite thermal conductivity is 2.4 W/m-K, over 400% higher than the 0.43 W/m-K value observed in this study. This is due to a number of limiting factors unique to thermal conductivity enhancement.

As discussed in section 2.5, the presence of a Kapitza resistance is the primary limiting factor in the property enhancement of thermal transport in nanocomposites [87] [93] [80] [101] [103] [112]. Imperfect filler-polymer contact is also cited as a deterrent to full exploitation of the filler modifier in conductivity enhancement [87] [93] [101] [105]. The fillers used in this study were not functionalized and, as observed through XRD testing discussed in section 4.1, no significant filler intercalation or exfoliation was achieved [113]. However, as complete filler exfoliation is not necessarily considered to be the ideal in thermal conductivity enhancement due to the reduced phonon scattering effect of filler-filler interfaces as compared to filler-matrix interfaces, the role of the imperfect or reduced filler-matrix contact in limiting thermal conductivity cannot be explored in this case [87] [93] [81].

The linear slope value of 5.7 W/m-K may be considered a net enhancement factor for the nanocomposite in this study after the effects of Kapitza and other limiting forces. By comparison to the thermal conductivity of the graphite nanofillers, it may also be possible to make an estimate of the interfacial thermal resistance. The idealized lowest possible thermal conductivity

case assumes unidirectional heat flow in the through-thickness filler direction of a fully aligned polymer nanocomposite as in Fig. 24 (a). In this case, of a maximum filler transport contribution of 6 W/m-K, the reduction factor may be quantified as 0.95 mK/W. In the idealized case of highest possible thermal conductivity, the uniaxial heat flow is in the in-plane direction of the filler modifiers such that 3,000 W/m-K is the filler transport contribution as in Fig. 24 (b). This leads to a reduction factor value of 1.9 x 10^{-3} mK/W. The filler contribution resulting in a 5.7 W/m-K being lower than the through-thickness intrinsic thermal conductivity of the filler modifier and several orders of magnitude lower than the in-plane filler conductivity illustrates the loss in thermal enhancement as a result of Kapitza resistance.

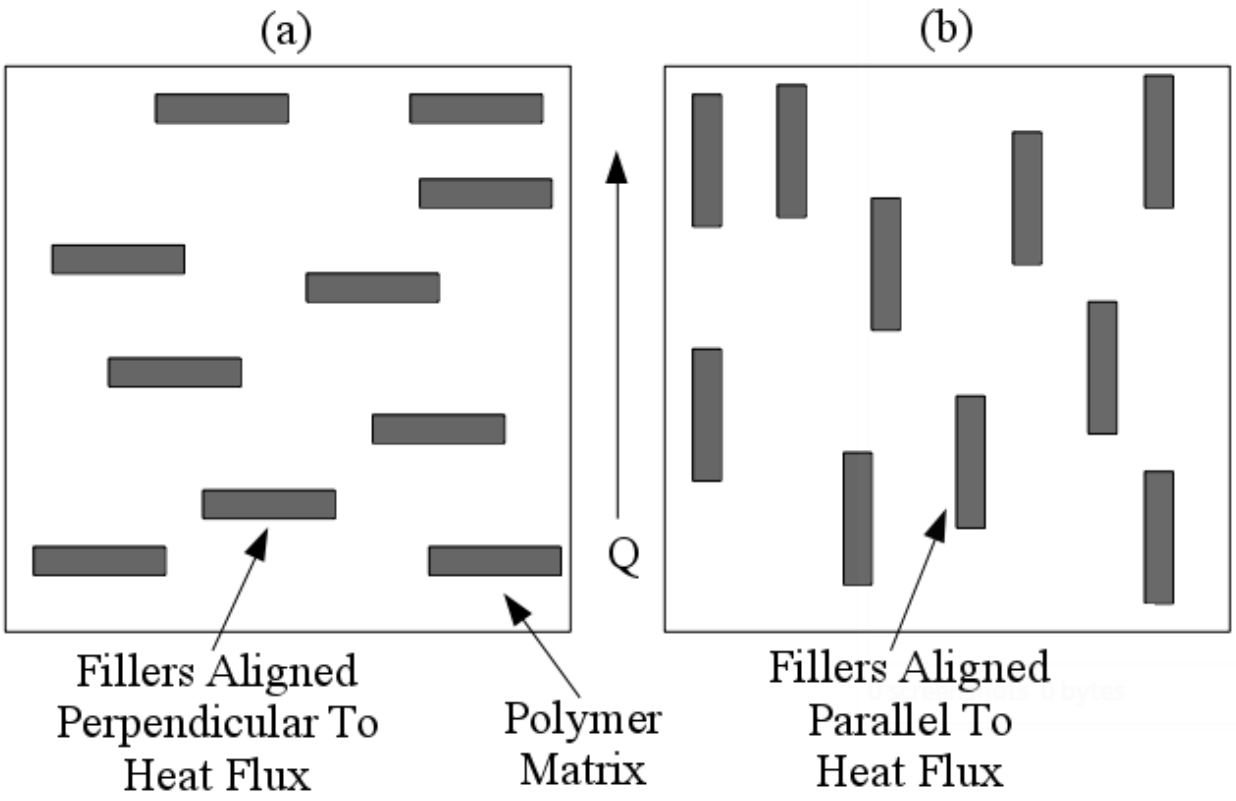

Figure 24 Idealized rule of mixtures comparison to experimental results

4.3 ANISOTROPIC ANALYSIS

The average volumetric heat capacities found for each of the specimen sets are presented in Table 2 below. Despite an overall increase in volumetric heat capacity due to the introduction of graphite filler modifiers, no significant trend was observed by increasing the amount of graphite nanoplatelets in the polymer nanocomposite.

Table 2 Average volumetric heat capacity values for PU-GNP nanocomposite at various filler loadings

Filler weight fraction (%wt)	Filler volume fraction (%vol)	Vol heat capacity (MJ/m^3K)
0%	0%	1.81
1%	14%	1.96
2%	25%	2.01
3%	33%	1.90
4%	40%	1.95

Strategic alignment of anisotropic filler modifiers, such as carbon nanotubes, as discussed in section 2.5, can lead to highly thermally conductive polymer nanocomposites due to the creation of quasi-percolating directional conductive networks [35] [87] [109] [93] [101] [105]. Although no alignment through processing or external force was intended in the fabrication of these polymer nanocomposites, anisotropic testing was performed, using the above values for average volumetric heat capacity, to quantify directional thermal conductivity due to the known highly anisotropic thermal transport properties of the graphite nanofiller [113]. The results of this analysis are shown in Fig. 25 below.

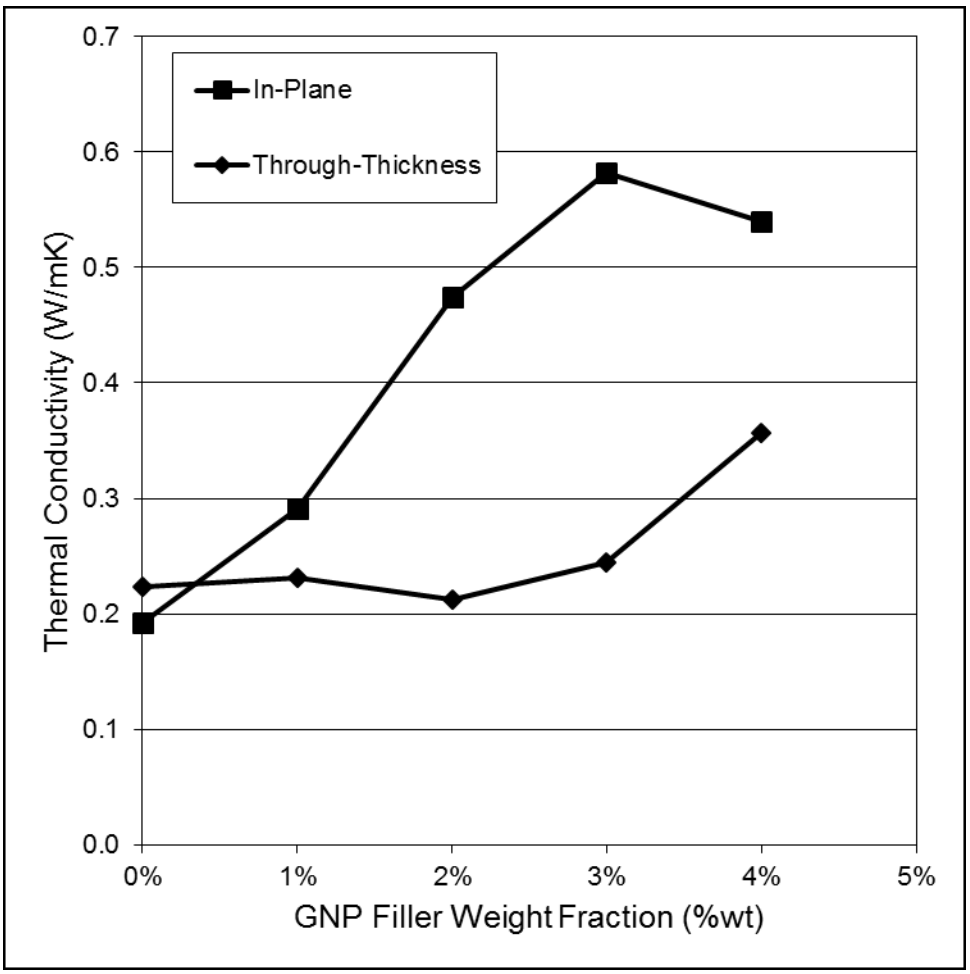

Figure 25 Directional thermal conductivity experimental data for PU-GNP nanocomposite at various filler loadings

Although the through-thickness thermal conductivity of the neat PU test specimens was found to be slightly higher than the in-plane conductivity, the material may be considered near isotropic. However, as filler content is introduced to the polymer, the in-plane thermal conductivity increases significantly above the through-thickness conductivity. Data from 1-3% filler weight fraction indicate a rapidly growing disparity between the directional conductivities. The through-thickness conductivity values, in fact, decrease below those recorded for the neat polymer, albeit not significantly. Previous studies have shown that nanocomposite thermal transport properties can degrade beyond the initial neat polymer values due to the introduction of the Kapitza resistance which may, in cases of low filler conductivity or content, have a net reducing effect on thermal conductivity [87] [80]. This is because the higher conductivity of the filler is unable to mitigate the effect of the low-efficiency interphase thermal transport thereby

causing the nanocomposite to behave as a hollow material in comparison to the neat single-phase polymer [87].

In this case, assuming a degree of in-plane alignment of the filler modifier, the lower through-thickness filler dimension of 6-8 nm and filler conductivity of 6 W/m-K, as compared to the in-plane diameter of 5 μm and conductivity of 3000 W/m-K, may explain the reduced value of through-thickness thermal conductivity observed for 2% filler weight fraction PU-GNP nanocomposite. This alignment condition may also result in the high conductivity observed in the in-plane direction, due to the higher efficiency afforded by the increased in-plane filler dimension and conductivity. The highest in-plane conductivity, recorded at 3% filler weight, of 0.58 W/m-K is significantly higher than its bulk counterpart of 0.36 W/m-K, as well as the 0.43 W/m-K bulk conductivity recorded for 4% filler weight fraction. As well, it is noted that, as shown in table 1 and Fig. 22, while thermal conductivity increases in a quasi-linear curve, the bulk conductivity improvement is slightly decreased from 2% to 3% filler volume. This is likely caused by the lack of improvement, or in some cases slight reduction, in the through-thickness conductivity which results in overall reduced transport through the test specimen, thus limiting the bulk conductivity of the nanocomposite.

At the highest 4% filler weight, the through-thickness conductivity increased while the in-plane conductivity sharply decreases reversing the previous trend. The bulk conductivity, shown in Table 1 and Fig. 22, is also increased at the highest rate between 3% and 4% filler weight fraction. Under the alignment assumption outlined above, this reversal in both bulk and anisotropic data would suggest that filler alignment is reduced in the 4% filler weight fraction nanocomposite. As the fabrication procedure was not altered in any way, this may be caused by increased filler content resulting in a more crowded internal filler-polymer arrangement as a maximum packing or saturation point is approached. At lower filler volume fractions, the graphite nanofillers may be permitted, by virtue of lower crowding, to settle in neat, arranged configurations at the base of the specimen prior to curing. This may be, in addition, to gravity, the result of solvent vaporization from the prepolymer-GNP-solvent mixture to cause the compatible prepolymer phase, to aggregate at the top of the plaque while the filler modifiers are aggregated to the bottom. This settlement-alignment hypothesis, shown below in Fig. 26 could explain the above results. To investigate the settlement and alignment of the specimens, further hot disk analysis and compression testing were performed.

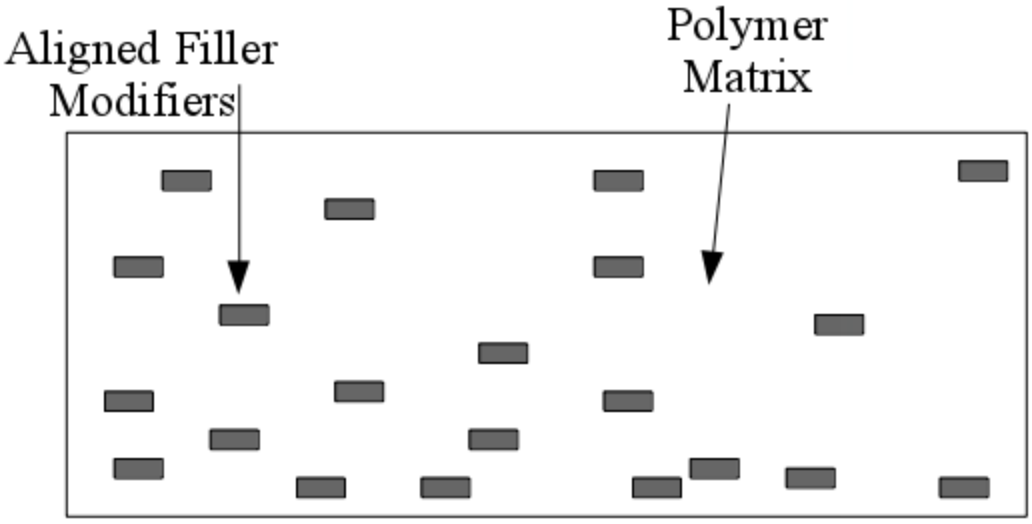

Figure 26 Hypothesized Internal Nanocomposite Structure

4.3.1 COMPRESSION TESTING

Figure 27 illustrates a single, representative linear compressive curve for a nanocomposite specimen in compression. The linear compressive modulus values obtained for axes A (through-thickness or axial), B, and C (in-plane or radial) through compressive testing to investigate filler alignment are shown below in Fig. 28.

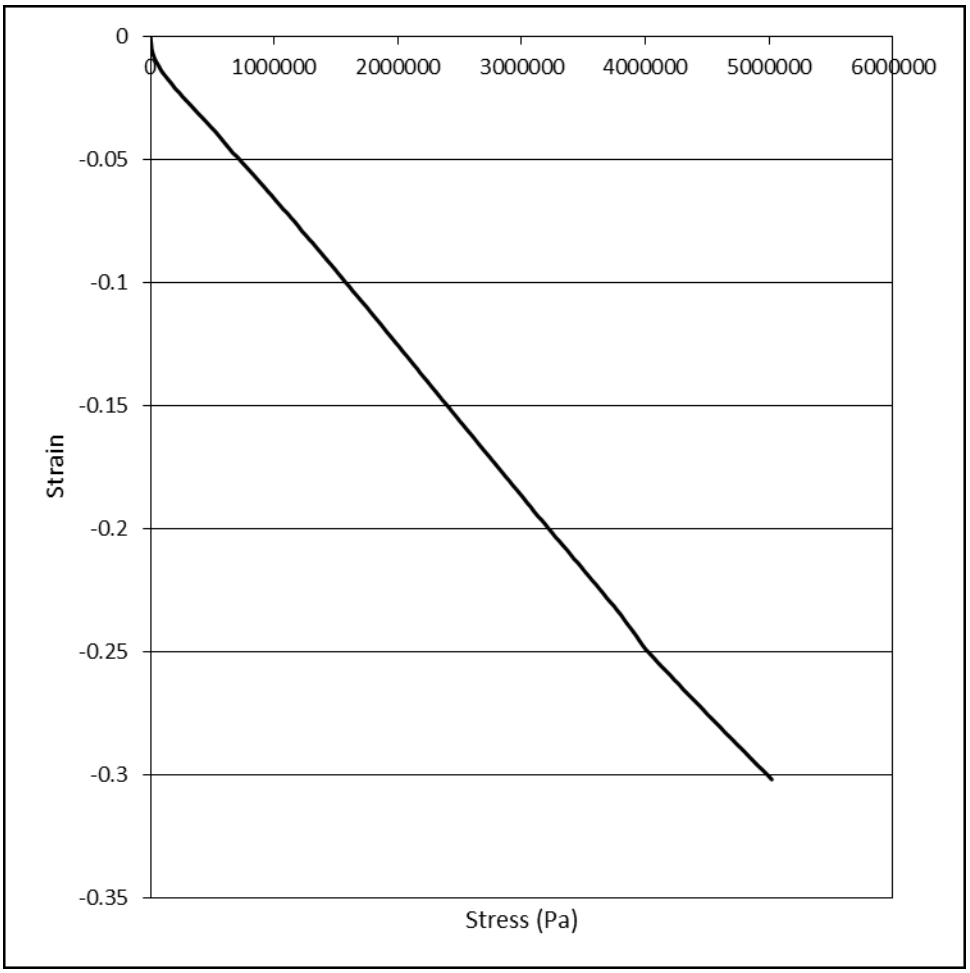

Figure 27 Stress (Pa)-Strain curve for 3% filler-modified PU nanocomposite under compression in the A (through-thickness) direction in its first test

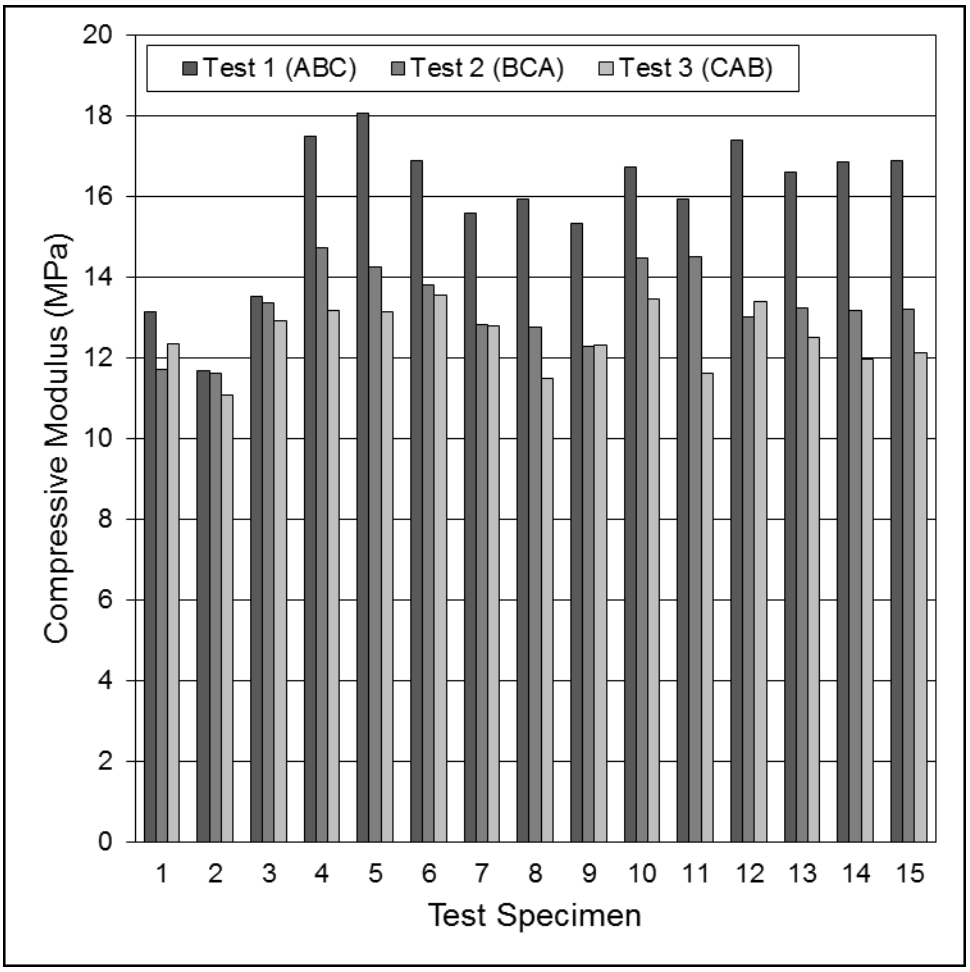

Figure 28 Compression testing results for PU-GNP nanocomposite at various filler loadings tested in multiple directions

The neat polymer values for each test, regardless of direction, are mostly uniform, in all three tests (1-3). Specimens 4-15, of modified nanocomposite specimens, are seen to possess a much higher compressive modulus in the first test, irrespective of direction. As in the case of volumetric heat capacity above, there is no discernable change caused by increasing filler modifier content, i. e. compressive modulus value of tests 4-7 with 1% filler weight fraction are comparable to modulus values of test 13-15 of 4% filler weight fraction nanocomposite. During the second and third tests, the modified nanocomposite compressive moduli are reduced to values very close to those observed in the neat polymer. To compare the compressive module in each of the three axes, therefore, directional values were plotted within test sets as shown in Fig. 29-31 below.

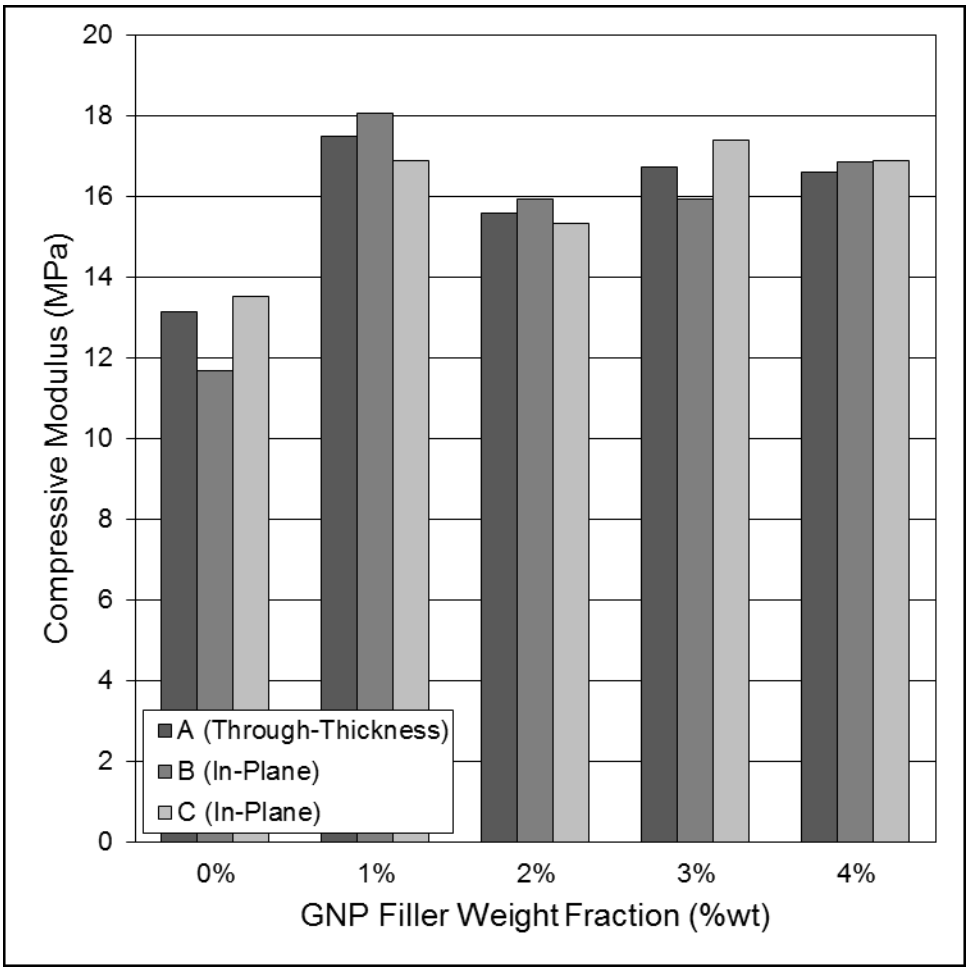

Figure 29 Test 1 compression results for PU-GNP nanocomposite at various filler loadings tested in multiple directions

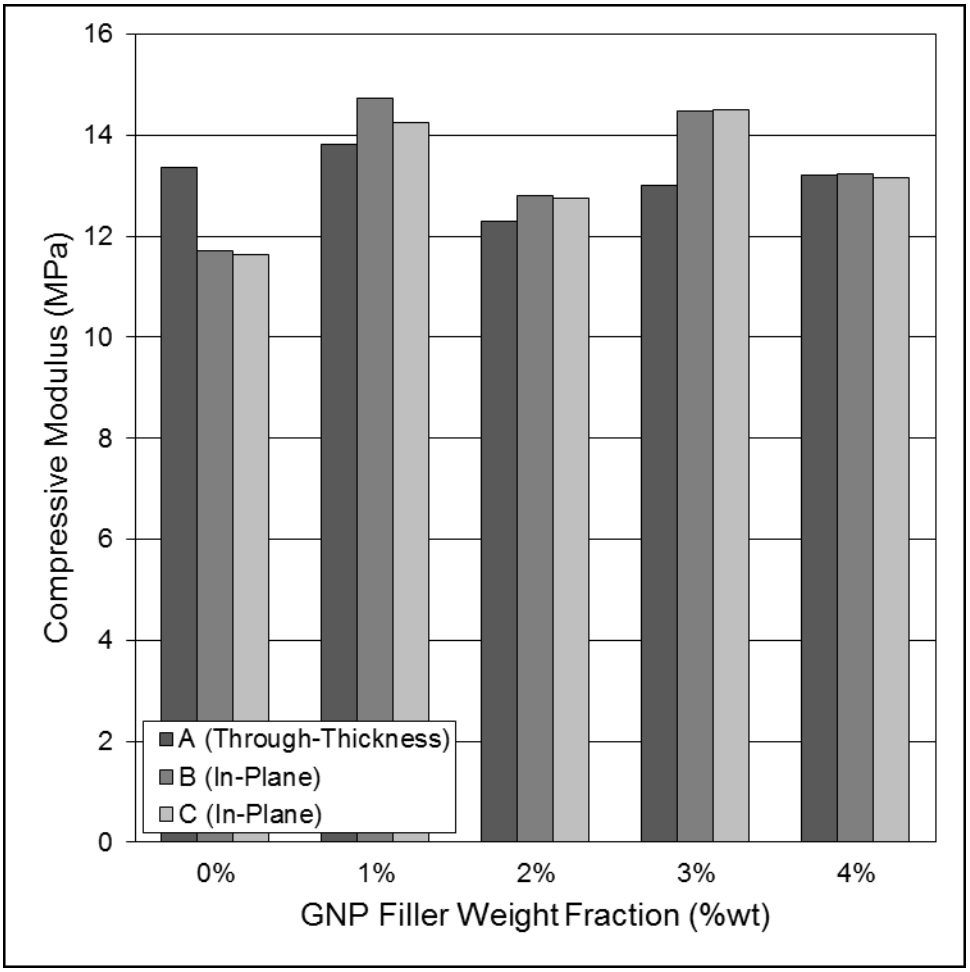

Figure 30 Test 2 compression results for PU-GNP nanocomposite at various filler loadings tested in multiple directions

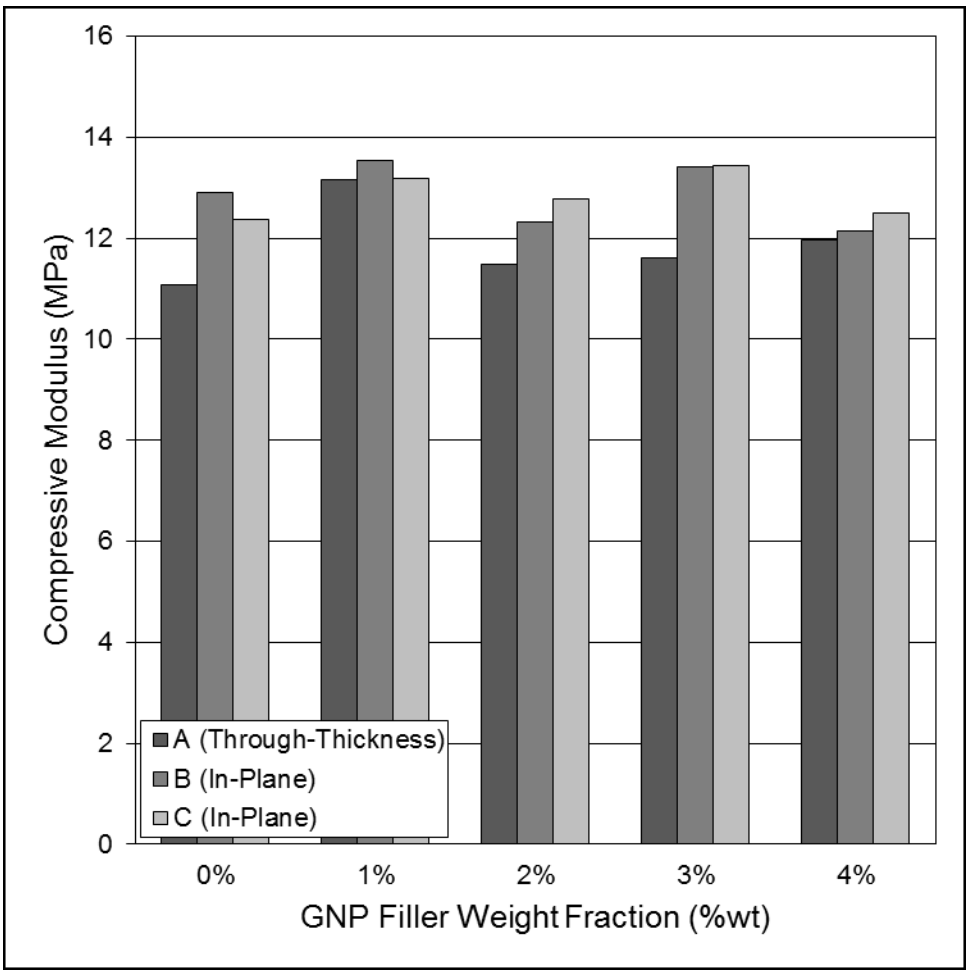

Figure 31 Test 3 compression results for PU-GNP nanocomposite at various filler loadings tested in multiple directions

Test 1 results, shown in Fig. 29, show no directional preference in any case. By comparison, results of tests two and three (Fig. 30 and Fig. 31, respectively) show lower A (through-thickness, axial) compressive moduli in all modified nanocomposites. As in Fig. 25 above, highest disparity is observed in 2% and 3% weight modified nanocomposite, while 4% weight filler weight fraction modified nanocomposite values are roughly equivalent in all three directions. However, it is also noted that the modified directional anisotropy does not often exceed the directional disparity observed in the presumably isotropic neat polymer in any of the tests and that the through-thickness compressive modulus is typically not the lowest value of the three directions in test 1. The change in compressive modulus, as well, due to filler addition is not as substantial as what is observed for thermal conductivity enhancement and therefore, the effect of alignment is not substantiated based on these compression testing results.

4.3.2 SETTLING

The ratios of in-plane to through-thickness thermal conductivity at various test settings, and hence probing depth, at various filler modifier concentrations are shown in Fig. 32 below. As indicated by Fig. 25, with the exception of 0% filler content PU, Fig. 32 shows higher in-plane conductivity in all cases. As the filler content is increased in-plane conductivity values far in excess of through-thickness values are observed peaking at 3% filler weight content. At 4% filler weight fraction, as expected from Fig. 25, the directional disparity of thermal conductivity is significantly reduced, though not fully eliminated. It may also be noted that in almost every case the lowest disparity between in-plane and through-thickness thermal conductivity values is observed at full axial probing depth while the highest is observed at half probing depth. This disagreement between the three test settings is increased from the 0% neat PU polymer to the 3% filler content nanocomposite and almost eliminated for the 4% filler-modified PU nanocomposite.

As previously discussed, these results show that the introduction and addition of filler modifiers rapidly enhances the in-plane thermal conductivity of the nanocomposite while either maintaining, or in some cases lowering, the original through-thickness thermal conductivity. Although this cannot be confirmed with the results of the compression testing, the in-plane bias observed here, regardless of probing depth, indicates some filler alignment in the in-plane direction. Additionally, the directional transport performance of the nanocomposite at limited probing depths heavily favors the in-plane direction until 4% filler weight addition. This added directional disagreement at lower depths suggests the presence of higher filler content at the base of the material, i. e. that some level of settling is occurring in the nanocomposite. Since thermal transport in the in-plane direction is heavily favored at lower probing depths, it may be concluded that the fillers at the base of the material are aligned in the in-plane direction. This alignment may have been induced by settling during nanocomposite fabrication.

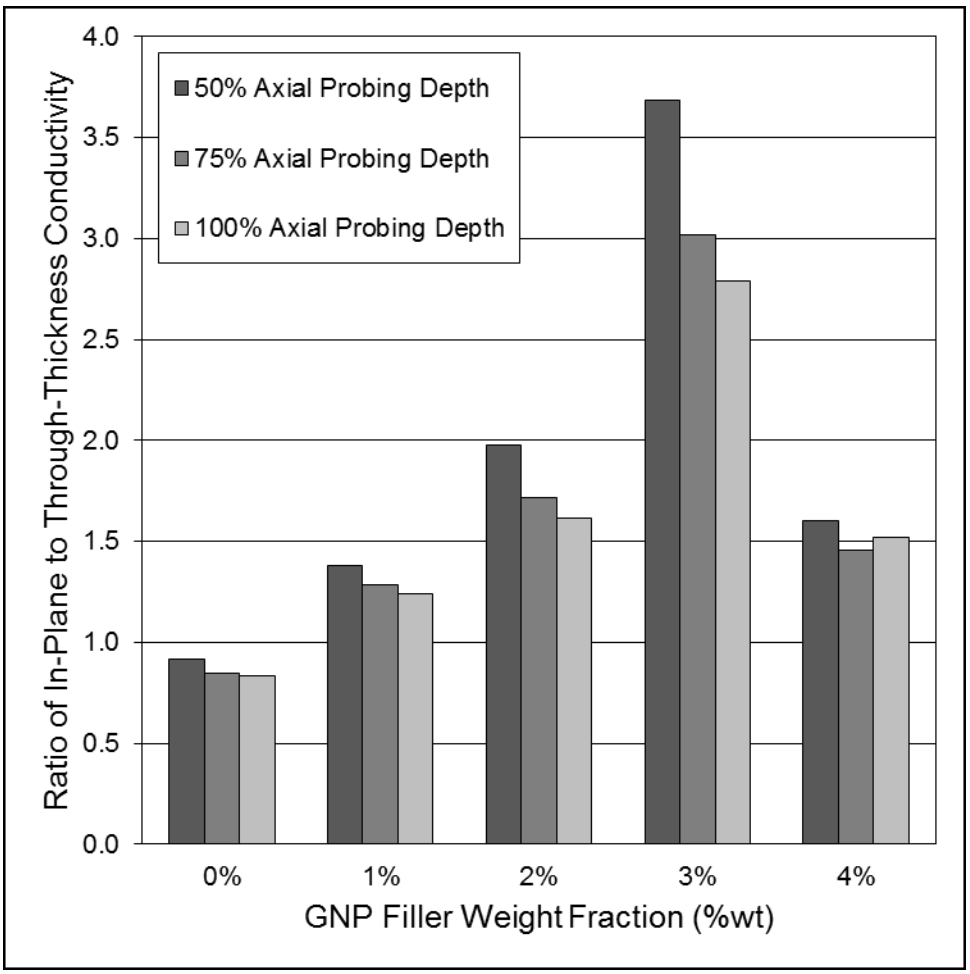

Figure 32 Ratio of in-plane to through-thickness thermal conductivity at various probing depths for PU-GNP nanocomposite at various filler loadings

Directional disparity is reduced at 75% and full probing depths, for 1-3% filler weight specimens, though it is not eliminated in any case. Filler alignment, therefore, is likely present, to some degree, throughout the specimens. At 4% filler weight (or 40% filler volume), the directional disagreement between various depths is virtually eliminated; however, the ratio of in-plane to through-thickness conductivity remains roughly 1.5 thus suggesting that while the settling-alignment has been reduced, it has not been fully eliminated and the material remains anisotropic. Although these results are not fully definitive, the compression and settling tests discussed above provide some evidence to support the settlement-alignment hypothesis outlined previously.

5. CONCLUSIONS

Highly engineered GNP filler modifier was added to PU polymer, using a solution blending method, at various filler weight fractions up to 4%, for thermal transport enhancement. GNP filler was found, through XRD analysis, to be poorly dispersed in the nanocomposite material. Results of bulk nanocomposite thermal conductivity measurement by hot disk analysis showed a linear thermal conductivity to filler weight fraction enhancement curve with no percolation, as expected from literature. Owing to the interfacial thermal or Kapitza resistance, caused by phonon mismatch between the matrix and filler phases, the overall enhancement effect of filler addition was far lower than what may be expected under the rule of mixtures model. Bulk data were however found to be in agreement with the series and other derivative analytical models when compared. Through curve fitting, the Nielsen and Maxwell second-order models were found to predict the thermal transport enhancement of this material system with good accuracy.

Specific heat capacity values, found through DSC, were used for anisotropic analysis of the thermal transport properties of the nanocomposite material. While the neat PU polymer was found to be mostly isotropic, thermal conductivity in the in-plane direction of the modified nanocomposite was much higher than in the through-thickness direction. For up to 3% filler weight fraction, while the in-plane conductivity increased to nearly 300% of the neat polymer conductivity, the through-thickness conductivity remained stagnant or was reduced slightly below the original through-thickness conductivity. Although the disparity between directional conductivities was still present in 4% filler weight fraction nanocomposite, it is sharply reduced along with the in-plane conductivity, as the through-thickness conductivity is increased.

Assuming the directional disparity to be caused by filler settling and alignment in the nanocomposite, the reversal at 4% filler weight may be attributed increased filler content preventing the GNP platelets from neatly settled in-plane aligned configurations. Through compression testing and further hot disk analysis settlement and alignment of filler modifiers was investigated. Results showed directional disparity is highest at lower probing depths in the nanocomposite specimens, which suggests filler settlement at the base of the specimen. Although the results of compression testing did not verify filler alignment, the in-plane bias in thermal transport at all probing depths suggests that filler alignment of the highly anisotropic high aspect

ratio filler modifiers was responsible for the directional disparity of the thermal conductivity in the nanocomposite material.

6. FUTURE WORK AND RECOMMENDATIONS

The thermal enhancement of polymer nanocomposites, as discussed in detail in this study, depends on a number of complex interconnected factors, the manipulation of which can drastically alter the final properties of the nanocomposite. Some of the options that may be explored to further investigate conductivity enhancement of PU polymer include the use of alternative fillers of various sizes and configurations at various degrees of filler addition and alternative nanocomposite fabrication methods [35] [87] [101] [105] [112] [77] [108] [101] [82] [108] [97].

Filler modifiers may be functionalized prior to fabrication to improve filler dispersion in order to examine in detail the effect of filler functionalization and dispersion in the polymer matrix as this relates to thermal enhancement [82] [83] [90] [91] [78] [40] [86]. Filler dispersion may also be manipulated during processing through, for instance, extended ultrasonication. Filler settling may be examined through extended observation of the prepolymer-filler mixture and controlled by the use of additives [129]. Filler alignment, to enhance the effect observed in this study, may be induced through processing or the application of external force during processing [35] [87] [109] [93] [101] [105]. Alignment may be further investigated by testing filler enhancement of electrical conductivity in multiple directions. Electrical testing may also prove useful in the comparison to thermal transport as it relates to percolation behavior.

The analysis of the nanocomposite internal structure may be extended through the use of methods such as Transmission Electron Microscopy [94] [38] [92] [95] [93] [37]. Macroscale testing of the nanocomposite, such as abrasive or tensile testing, may be attempted to investigate any positive or negative unforeseen effects of filler addition on material performance and longevity.

REFERENCES

[1] J. Rösler, H. Harders and M. Bäker, "1. The structure of materials," in *Mechanical Behaviour of Engineering Materials: Metals, Ceramics, Polymers, and Composites*, New York, Springer, 2007, pp. 1-25.

[2] D. Sekhar Bag, "Chapter 1 - General Introduction," in *Principles of Polymers : An Advanced Book*, New York, Nova Publishers, 2013, pp. 1-29.

[3] J. W. Nicholson, "Chapter 1. Polymer Chemistry," in *The Chemistry of Polymers: 3rd Edition*, Dorchester, RSC Publishing, 2006, pp. 1-21.

[4] D. Braun, H. Cherdron, M. Rehahn, H. Ritter and B. Voit, "1. Introduction," in *Polymer Synthesis: Theory and Practice – Fundamentals, Methods, Experiments*, Berlin, Springer, 2013, pp. 1-30.

[5] J. Rösler, H. Harders and M. Bäker, "8. Mechanical behaviour of polymers," in *Mechanical Behaviour of Engineering Materials: Metals, Ceramics, Polymers, and Composites*, New York, Springer, 2007, pp. 257-292.

[6] D. Sekhar Bag, "Chapter 2 - Polymerization And Polymerization Processes," in *Principles of Polymers : An Advanced Book*, New York, Nova Publishers, 2013, pp. 31-61.

[7] M. Chanda and S. K. Roy, "1. Industrial Polymers," in *Industrial Polymers, Specialty Polymers, and Their Applications*, Boca Raton, CRC Press, 2009, pp. 1.1-1.159.

[8] J. W. Nicholson, "Chapter 3. Polymer Structure," in *The Chemistry of Polymers: 3rd Edition*, Dorchester, RSC Publishing, 2006, pp. 40-53.

[9] J. W. Nicholson, "Chapter 4. Crosslinking," in *The Chemistry of Polymers: 3rd Edition*, Dorchester, RSC Publishing, 2006, pp. 54-63.

[10] M. Špérová, P. Nasadil, A. Průšová and J. Kučerík, "A hint on the correlation between cellulose fibers polymerization degree and their thermal and thermo-oxidative degradation," *Journal of Thermal Analysis & Calorimetry,* vol. 110, no. 1, pp. 71-76, 2012.

[11] Y.-Y. Wang, T. Yang, M. Tian and R.-J. Liao, "THE RELATIONSHIP BETWEEN DP, FRACTURE DEGREE AND MECHANICAL STRENGTH OF CELLULOSE Iβ IN INSULATION PAPER BY MOLECULAR DYNAMIC SIMULATIONS," *International Journal of Modern Physics B: Condensed Matter Physics; Statistical Physics; Applied Physics,* vol. 27, no. 31, pp. 1-11, 2013.

[12] M. Chanda and S. K. Roy, "2. Polymers in Special Uses," in *Industrial Polymers, Specialty Polymers, and Their Applications*, Boca Raton, CRC Press, 2009, pp. 2.1-2.155.

[13] Y. Deng, C.-S. Zhao and Y.-Z. Wang, "Effects of phosphorus-containing thermotropic liquid crystal copolyester on pyrolysis of PET and its flame retardant mechanism," *Polymer Degradation & Stability,* vol. 93, no. 11, pp. 2066-2070, 2008.

[14] J. W. Nicholson, "Chapter 10. Special Topics in Polymer Chemistry," in *The Chemistry of Polymers: 3rd Edition*, Dorchester, RSC Publishing, 2006, pp. 146-158.

[15] S. Sanchez-Valdes, "Influence of maleated elastomer on filler dispersion, mechanical and antimicrobial properties of hybrid HDPE/clay/silver nanocomposites," *Journal of Adhesion Science & Technology,* vol. 30, no. 9, pp. 1006-1016, 2016.

[16] S. Thomas, K. Joseph, S. K. Malhotra, K. Goda and M. S. Sreekala, "Advances in Polymer Composites: Macro- and Microcomposites – State of the Art, New Challenges, and Opportunities," in *Polymer Composites: Volume 1*, Weinheim, Wiley-VCH, 2012, pp. 3-16.

[17] P. Deepalekshmi, P. M. Visakh, A. P. Mathew, A. K. Chandra and S. Thomas, "Advances in Elastomers: Their Composites and Nanocomposites: State of Art, New Challenges and Opportunities," in *Advances in Elastomers II Composites and Nanocomposites*, Berlin,

Springer, 2013, pp. 1-10.

[18] V. R. Arun Prakash and A. Rajadurai, "MECHANICAL, THERMAL AND DIELECTRIC CHARACTERIZATION OF IRON OXIDE PARTICLES DISPERSED GLASS FIBER EPOXY RESIN HYBRID COMPOSITE," *Digest Journal of Nanomaterials & Biostructures,* vol. 11, no. 2, pp. 373-380, 2016.

[19] J. Rösler, H. Harders and M. Bäker, "9. Mechanical behaviour of fibre reinforced composites," in *Mechanical Behaviour of Engineering Materials: Metals, Ceramics, Polymers, and Composites*, New York, Springer, 2007, pp. 295-325.

[20] Funk & Wagnalls New World Encyclopedia, *Composite Material,* N/A: World Almanac Education Group, 2014.

[21] M. Kumaresan, S. Sathish and N. Karthi, "Effect of Fiber Orientation on Mechanical Properties of Sisal Fiber Reinforced Epoxy Composites," *Journal of Applied Science and Engineering,* vol. 18, no. 3, pp. 289-294, 2015.

[22] S. Naseva, V. Srebrenkoska, S. Risteka, M. Stefanovska and S. Srebrenkoska, "MECHANICAL PROPERTIES OF FILAMENT WOUND PIPES: EFFECTS OF WINDING ANGLES," *Quality of Life: A Multi-Disciplinary Journal of Food Science, Environmental Science & Public Health,* vol. 6, no. 1-2, pp. 10-15, 2015.

[23] S. Thomas, K. Joseph, S. K. Malhotra, K. Goda and M. S. Sreekala, "Applications of Macro- and Microfiller-Reinforced Polymer Composites," in *Polymer Composites: Volume 1*, Weinheim, Wiley-VCH, 2012, pp. 749-772.

[24] Q. Liu and J. Paavola, "Lightweight design of composite laminated structures with frequency constraint," *Composite Structures,* vol. N/A, no. N/A, p. N/A, 2015.

[25] M. Mohamed, S. Hawkins and K. Chandrashekhara, "Manufacturing and Performance Evaluation of Polyurethane Composites Using One-part and Two-part Resin Systems," *Polymers & Polymer Composites,* vol. 23, no. 5, pp. 333-344, 2015.

[26] M. Hosur, S. Waliul Islam, U. Vaidya, A. Kumar, P. Dutta and S. Jeelani, "Dynamic punch shear characterization of plain weave graphite/epoxy composites at room and elevated temperatures," *Composite Structures,* vol. 70, no. 3, pp. 295-307, 2005.

[27] K. Ogi, T. Nishikawa, Y. Okano and I. Taketa, "Mechanical properties of ABS resin reinforced with recycled CFRP," *Advanced Composite Materials,* vol. 16, no. 2, pp. 181-194, 2007.

[28] R. Atif, I. Shyha and F. Inam, "Mechanical, Thermal, and Electrical Properties of Graphene-Epoxy Nanocomposites-A Review," *Polymers,* vol. 8, no. 8, pp. 1-37, 2016.

[29] L. Sutherland and C. G. Soares, "Contact indentation of marine composites," *Composite Structures,* vol. 70, no. 3, pp. 287-294, 2005.

[30] R. Azadi and Y. Rostamiyan, "Experimental and analytical study of buckling strength of new quaternary hybrid nanocomposite using Taguchi method for optimization," *Construction & Building Materials,* vol. 88, no. N/A, pp. 212-224, 2015.

[31] G. Yongchang, L. Lijuan, D. Jun and Z. Genquan, "The Influence of Hollow Imperfections of Adhesive on Performances of Interface of RC Beams Strengthened with HFRP.," in *AIP Conference Proceedings*, 2010.

[32] Y.-l. Yang, J.-w. Liu and G.-j. Xiong, "Flexural behavior of wood beams strengthened with HFRP," *Construction & Building Materials,* vol. 43, no. N/A, pp. 118-124, 2013.

[33] G.-I. Shim, S.-H. Kim, D.-L. Ahn, J.-K. Park, D.-H. Jin, D.-T. Chung and S.-Y. Choi, "Experimental and numerical evaluation of transparent bulletproof material for enhanced impact-energy absorption using strengthened-glass/polymer composite," *Composites: Part B, Engineering,* vol. 97, no. N/A, pp. 150-161, 2016.

[34] E. Zeimaran, S. Pourshahrestani, B. Pingguan-Murphy, N. Kadri, H. Rothan, R. Yusof, M. Towler and I. Djordjevic, "Fabrication and characterization of poly(octanediol citrate)/gallium-containing bioglass microcomposite scaffolds," *Journal of Materials*

Science, vol. 50, no. 5, pp. 2189-2201, 2015.

[35] T. P. Nguyen, "Applications of Polymer-Based Nanocomposites," in *Polymer composites: Volume 2*, Weinheim, Wiley-VCH, 2013, pp. 249-278.

[36] Q. Zhao, H. Chen and B. Yao, "An analytic interfacial stresses solution of simply supported HFRP beam under uniformly distributed loading," *Composite Interfaces,* vol. 14, no. 1, pp. 33-47, 2007.

[37] M. V. Hosur, "Enhancement of Thermal, Thermomechanical, and Mechanical Properties of Carbon-Fiber-Reinforced and Sandwich Composites Through Nanophased Epoxy/Foam," in *Recent Advances in Polymer Nanocomposites*, Boca Raton, CRC Press, 2009, pp. 285-336.

[38] L. Wang, J. Li, R. Hong and H. Li, "Synthesis, Surface Modification, and Characterization of Nanoparticles," in *Polymer composites: Volume 2*, Weinheim, Wiley-VCH, 2013, pp. 13-52.

[39] F. Lionetto, E. Calò, F. Di Benedetto, D. Pisignano and A. Maffezzoli, "A methodology to orient carbon nanotubes in a thermosetting matrix," *Composites Science & Technology,* vol. 96, no. N/A, pp. 47-55, 2014.

[40] K. A. Iyer, J. Lechanski and J. M. Torkelson, "Green polypropylene/waste paper composites with superior modulus and crystallization behavior: Optimizing specific energy in solid-state shear pulverization for filler size reduction and dispersion," *Composites: Part A, Applied Science & Manufacturing,* vol. 83, no. N/A, pp. 47-55, 2016.

[41] P. Kumar, K. P. Sandeep, S. Alavi and V. D. Truong, "A Review of Experimental and Modeling Techniques to Determine Properties of Biopolymer-Based Nanocomposites," *Journal of Food Science,* vol. 76, no. 1, pp. E2-E14, 2011.

[42] G. Qi, B. Zhang and Y. Yu, "Research on carbon fiber/epoxy interfacial bonding characterization of transverse fiber bundle composites fabricated by different preparation

processes: Effect of fiber volume fraction.," *Polymer Testing,* vol. 52, no. N/A, pp. 150-156, 2016.

[43] L. I. Cavaco and J. A. Melo, "Preface," in *Polyurethane: Properties, Structure and Applications*, New York, Nova Science Publishers, 2012, pp. vii-xi.

[44] H. Ashrafizadeh, A. McDonald and P. Mertiny, "Deposition of Electrically Conductive Coatings on Castable Polyurethane Elastomers by the Flame Spraying Process," *Journal of Thermal Spray Technology,* vol. 25, no. 3, pp. 419-430, 2016.

[45] P. Król, "Chapter One Introduction," in *Linear polyurethanes: synthesis methods, chemical structures, properties and applications*, Leiden, VSP, 2008, pp. 1-5.

[46] J. B. de Oliveira, L. G. T. dos Reis and F. S. Semaan, "POLYURETHANES IN ANALYTICAL CHEMISTRY: A MYRIAD OF APPLICATIONS FROM SORBENT FOAMS TO CONDUCTIVE MATERIALS AND SENSORS," in *Polyurethane: Properties, Structure and Applications*, New York, Nova Science Publishers, 2012, pp. 1-23.

[47] T. Thomson, "2 Polyurethane Chemistry in Brief," in *Polyurethanes as specialty chemicals: principles and applications*, Boca Raton, CRC Press, 2005, p. N/A.

[48] K. Ashida, "Chapter Two Historical Developments of Polyurethane and Polyisocyanurate Foams," in *Polyurethane and related foams: chemistry and technology*, Boca Raton, CRC, 2007, pp. 5-10.

[49] I. Clemitson, "Chapter 1 - Introduction," in *Polyurethane casting primer*, Boca Raton, CRC Press, 2012, pp. 1-9.

[50] Y. Wang, Z. Sun, J. Tian, H. Wang, H. Wang and Y. Ji, "Influence of Environment on Ageing Behaviour of the Polyurethane Film," *Materials Science,* vol. 22, no. 2, pp. 290-294, 2016.

[51] H. M. C. Chathuranga Somarathna, S. N. Raman, K. H. Badri, A. A. Mutalib, D. Mohotti and S. D. Ravana, "Quasi-Static Behavior of Palm-Based Elastomeric Polyurethane: For Strengthening Application of Structures under Impulsive Loadings," *Polymers,* vol. 8, no. 5, pp. 1-20, 2016.

[52] D. G. L. a. P. Cranley, "Polyurethane Adhesives," in *Handbook of Adhesive Technology, Revised and Expanded*, vol. New York, New York, CRC Press, 2003, pp. 695-718.

[53] R. Zhou, D. Lu, Y. Jiang and Q. Li, "Mechanical properties and erosion wear resistance of polyurethane matrix composites," *Wear,* vol. 259, no. 1-6, pp. 676-683, 2005.

[54] I. R. Clemitson, "2 Chemistry of Polyurethanes," in *Castable Polyurethane Elastomers*, Boca Raton, CRC Press, 2015, pp. 13-44.

[55] W. Sakulsaknimitr, S. Wirasate, K. Pipatpanyanugoon and P. Atorngitjawat, "Structure and Thermal Properties of Polyurethanes Synthesized from Cardanol Diol," *Journal of Polymers & the Environment,* vol. 23, no. 2, pp. 216-226, 2015.

[56] M. ŠERCER, P. RAOS and M. RUJNIĆ-SOKELE, "STUDY ON THERMAL PROPERTIES OF SYNTHETIC AND BIO-BASED POLYURETHANE," *Thermal Science,* vol. 19, no. 3, pp. 915-922, 2015.

[57] E. Orgilés-Calpena, F. Arán-Aís, A. M. Torró-Palau and C. Orgilés-Barceló, "Sustainable Polyurethane Adhesives Derived From Carbon Dioxide," *Polymers from Renewable Resources,* vol. 7, no. 1, pp. 1-12, 2016.

[58] N. Cuinat-Guerraz, M.-J. Dumont and P. Hubert, "Environmental resistance of flax/bio-based epoxy and flax/polyurethane composites manufactured by resin transfer moulding," *Composites: Part A, Applied Science & Manufacturing,* vol. 88, no. N/A, pp. 140-147, 2016.

[59] K. Ashida, "Chapter One Introduction," in *Polyurethane and related foams: chemistry and*

technology, Boca Raton, CRC, 2007, pp. 1-3.

[60] K. Ashida, "Chapter Three Fundamentals," in *Polyurethane and related foams: chemistry and technology*, Boca Raton, CRC, 2007, pp. 11-64.

[61] I. Clemitson, "Chapter 2 – Fundamentals," in *Polyurethane casting primer*, Boca Raton, CRC Press, 2012, pp. 11-31.

[62] M. Szycher, "Structure–Property Relations in Polyurethanes," in *Szycher's handbook of polyurethanes*, Boca Raton, CRC Press, 2012, pp. 37-86.

[63] P. Król, "Chapter Two Basic Raw Materials For The Production Of Linear Polyurethanes," in *Linear polyurethanes: synthesis methods, chemical structures, properties and applications*, Leiden, VSP, 2008, pp. 7-16.

[64] M. Szycher, "Basic Concepts in Polyurethane Chemistry and Technology," in *Szycher's handbook of polyurethanes*, Boca Raton, CRC Press, 2012, pp. 13-36.

[65] I. R. Clemitson, "8 Properties," in *Castable Polyurethane Elastomers*, Boca Raton, CRC Press, 2015, pp. 161-191.

[66] M. Szycher, "Introduction," in *Szycher's handbook of polyurethanes*, Boca Raton, CRC Press, 2012, pp. 1-12.

[67] I. R. Clemitson, "9 Applications," in *Castable Polyurethane Elastomers*, Boca Raton, CRC Press, 2015, pp. 193-210.

[68] Q. Tian, I. Krakovský, G. Yan, L. Bai, J. Liu, G. Sun, L. Rosta, B. Chen and L. Almásy, "Microstructure Changes in Polyester Polyurethane upon Thermal and Humid Aging," *Polymers,* vol. 8, no. 5, pp. 1-12, 2016.

[69] I. A. Novakov, M. A. Vaniev, D. Medvedev, N. V. Sidorenko, G. V. Medvedev and D. O. Gusev, "THERMAL STABILITY OF ELASTIC POLYURETHANE," in *Materials*

science of polymers: plastics, rubber, blends, and composites, Toronto, Apple Academic Press, 2015, pp. 145-154.

[70] H. Ashrafizadeh, A. McDonald and P. Mertiny, "DEVELOPMENT OF A TEST ASSEMBLY FOR EVALUATING THE EROSION RESISTANCE OF POLYURETHANE ELASTOMERS AT CONTROLLED TEMPERATURES," in *Proceedings of the First Pacific Rim Thermal Engineering Conference*, Hawaii, 2016.

[71] N. Zhang, F. Yang, L. Li, C. Shen, J. Castro and L. J. Lee, "Thickness effect on particle erosion resistance of thermoplastic polyurethane coating on steel substrate," *Wear,* vol. 303, no. 1/2, pp. 49-55, 2013.

[72] L. M. Jiji, "Basic Concepts," in *Heat Conduction*, Berlin, Springer, 2009, pp. 1-23.

[73] I. R. Clemitson, "1 Introduction to Polyurethanes," in *Castable Polyurethane Elastomers*, Boca Raton, CRC Press, 2015, pp. 1-8.

[74] M. Rogulska, A. Kultys and J. Lubczak, "New thermoplastic polyurethane elastomers based on aliphatic-aromatic chain extenders with different content of sulfur atoms," *Journal of Thermal Analysis & Calorimetry,* vol. 121, no. 1, pp. 397-410, 2015.

[75] Q. Jing, Q. Liu, L. Li, Z. Dong and V. V. Silberschmidt, "Effect of graphene-oxide enhancement on large-deflection bending performance of thermoplastic polyurethane elastomer," *Composites: Part B, Engineering,* vol. 89, no. N/A, pp. 1-8, 2016.

[76] M. Szycher, "Elastomers," in *Szycher's handbook of polyurethanes*, Boca Raton, CRC Press, 2012, pp. 345-372.

[77] M. Oliveira and A. V. Machado, "Preparation of Polymer-Based Nanocomposites by Different Routes," in *Nanocomposites: synthesis, characterization and applications*, Hauppauge, Nova Science Publishers, Inc, 2011, pp. 73-94.

[78] Q. Zeng and A. Yu, "Theory and Simulation in Nanocomposites," in *Polymer composites:*

Volume 2, Weinheim, Wiley-VCH, 2013, pp. 53-74.

[79] C. I. Idumah and A. Hassan, "Recently emerging trends in thermal conductivity of polymer nanocomposites," *Review in Chemical Engineering,* vol. 32, no. 4, pp. 413-457, 2016.

[80] A. Kausar, Z. Anwar and B. Muhammad, "Recent Developments in Epoxy/Graphite, Epoxy/Graphene, and Epoxy/Graphene Nanoplatelet Composites: A Comparative Review," *Polymer-Plastics Technology & Engineering,* vol. 55, no. 11, pp. 1192-1210, 2016.

[81] W. Evans, R. Prasher, J. Fish, P. Meakin, P. Phelan and P. Keblinski, "Effect of aggregation and interfacial thermal resistance on thermal conductivity of nanocomposites and colloidal nanofluids," *International Journal of Heat and Mass Transfer,* vol. 51, no. N/A, pp. 1431-1438, 2008.

[82] N. Q. Khuyen, B. S. Kim, J. H. Byun and S. Lee, "Mechanical Properties of VGCF/MAPP and Atmospheric Plasma-Treated VGCF/PP by Melt-Mixing Process," *Advanced Composite Materials,* vol. 19, no. 4, pp. 381-392, 2010.

[83] D. Kotnarowska, M. Przerwa and T. Szumiata, "Resistance to Erosive Wear of Epoxy-Polyurethane Coating Modified With Nanofillers," *Quarterly Journal of Austrian Economics,* vol. 3, no. 2, pp. 52-58, 2014.

[84] X. Zheng, J. Fontana, M. Pevnyi, M. Ignatenko, S. Wang, R. Vaia and P. Palffy-Muhoray, "The effects of nanoparticle shape and orientation on the low frequency dielectric properties of nanocomposites," *Journal of Materials Science,* vol. 47, no. 12, pp. 4914-4920, 2012.

[85] R. Kotsilkova, E. Ivanov, D. Bychanok, A. Paddubskaya and P. Kuzhir, "Effect of Matrix Viscosity on Rheological and Microwave Properties of Polymer Nanocomposites with Multiwall Carbon Nanotubes," *Journal of Theoretical & Applied Mechanics,* vol. 44, no. 2, pp. 83-96, 2014.

[86] R. Taherian, "Experimental and analytical model for the electrical conductivity of polymer-based nanocomposites," *Composites Science & Technology,* vol. 123, no. N/A, pp. 17-31, 2016.

[87] Z. Han and A. Fina, "Thermal conductivity of carbon nanotubes and their polymer nanocomposites: A review," *Progress in Polymer Science,* vol. 36, no. 7, pp. 914-944, 2011.

[88] A. Naz, A. Kausar and M. Siddiq, "Influence of Graphite Filler on Physicochemical Characteristics of Polymer/Graphite Composites: A Review," *Polymer-Plastics Technology & Engineering,* vol. 55, no. 6, pp. 604-625, 2016.

[89] R. K. Gupta, E. B. Kennel and K.-J. Kim, "Overview of Challenges and Opportunities," in *Polymer Nanocomposites Handbook*, Boca Raton, CRC Press, 2010, pp. 1-6.

[90] H. C. Ashton, "The Incorporation of Nanomaterials into Polymer Media," in *Polymer Nanocomposites Handbook*, Boca Raton, CRC Press, 2010, pp. 21-44.

[91] R. Y. Hong, H. P. Fu, Y. J. Zhang, L. Liu, J. Wang, H. Z. Li and Y. Zheng, "Surface-modified silica nanoparticles for reinforcement of PMMA," *Journal Of Applied Polymer Science,* vol. 105, no. 4, pp. 2176-2184, 2007.

[92] L. Wang, K. Wang, L. Chen, Y. Zhang and C. He, "Preparation, morphology and thermal/mechanical properties of epoxy/nanoclay composite," *Composites: Part A, Applied Science & Manufacturing,* vol. 37, no. 11, pp. 1890-1896, 2006.

[93] A. Patti, P. Russo, D. Acierno and S. Acierno, "The effect of filler functionalization on dispersion and thermal conductivity of polypropylene/multi wall carbon nanotubes composites," *Composites: Part B, Engineering,* vol. 94, no. N/A, pp. 350-359, 2016.

[94] A. Saritha, S. K. Malhotra, S. Thomas, K. Joseph, K. Goda and M. S. Sreekala, "State of the Art – Nanomechanics," in *Polymer composites: Volume 2*, Weinheim, Wiley-VCH,

2013, pp. 1-12.

[95] B. E. Smith, H. Yazdani and K. Hatami, "Three-dimensional imaging and quantitative analysis of dispersion and mechanical failure in filled nanocomposites," *Composites: Part A, Applied Science & Manufacturing,* vol. 79, no. N/A, pp. 23-29, 2015.

[96] G. V. Kozlov, Y. G. Yanovskii and G. E. Zaikov, "Modern Experimental and Theoretical Analysis Methods of Particulate-Filled Nanocomposites Structure," in *Modeling and prediction of polymer nanocomposite properties*, Weinheim, Wiley-VCH, 2013, pp. 39-62.

[97] G. Pircheraghi, R. Foudazi and I. Manas-Zloczower, "Characterization of carbon nanotube dispersion and filler network formation in melted polyol for nanocomposite materials," *Powder Technology,* vol. 276, no. N/A, pp. 222-231, 2015.

[98] W. Steinmann, T. Vad, B. Weise, J. Wulfhorst, G. Seide, T. Gries, M. Heidelmann and T. Weirich, "Extrusion of CNT-modified Polymers With Low Viscosity - Influence of Crystallization and CNT Orientation on the Electrical Properties," *Polymers & Polymer Composites,* vol. 21, no. 8, pp. 473-481, 2013.

[99] C. Dinh Van and T. Dinh Van, "The MEH-PPV/YAG:Ce Hybrid Nanocomposite Material for Solution Processing Fabrication of Optoelectronic Device," *Journal of Nanomaterials,* vol. 2015, no. N/A, pp. 1-5, 2015.

[100] S. Y. Kim, Y. J. Noh and J. Yu, "Thermal conductivity of graphene nanoplatelets filled composites fabricated by solvent-free processing for the excellent filler dispersion and a theoretical approach for the composites containing the geometrized fillers," *Composites: Part A, Applied Science & Manufacturing,* vol. 69, no. N/A, pp. 219-225, 2015.

[101] A. Naz, A. Kausar, M. Siddiq and M. A. Choudhary, "Comparative Review on Structure, Properties, Fabrication Techniques, and Relevance of Polymer Nanocomposites Reinforced with Carbon Nanotube and Graphite Fillers," *Polymer-Plastics Technology & Engineering,* vol. 55, no. 2, pp. 171-198, 2016.

[102] W. Benhadjala, M. Gravoueille, I. Bord-Majek, L. Béchou, E. Suhir, M. Buet, M. Louarn, M. Weiss, F. Rougé, V. Gaud and Y. Ousten, "Inorganic/organic nanocomposites: Reaching a high filler content without increasing viscosity using core-shell structured nanoparticles," *Applied Physics Letters,* vol. 107, no. 21, pp. 1-4, 2015.

[103] M. Wang, D. Galpaya, Z. B. Lai, Y. Xu and C. Yan, "Surface functionalization on the thermal conductivity of graphene–polymer nanocomposites," *International Journal of Smart & Nano Materials,* vol. 5, no. 2, pp. 123-132, 2014.

[104] C. A. Stergiou, A. Z. Stimoniaris and C. G. Delides, "Hybrid Nanocomposites With Organoclay and Carbon-Based Fillers for EMI Suppression," *IEEE Transactions on Electromagnetic Compatibility,* vol. 57, no. 31, pp. 470-476, 2015.

[105] S. Agarwal and R. K. Gupta, "Thermal Conductivity of Polymer Nanocomposites," in *Polymer Nanocomposites Handbook*, Boca Raton, CRC Press, 2010, pp. 485-512.

[106] J. Guo, J. Chen and E. Pan, "Analytical three-dimensional solutions of anisotropic multilayered composite plates with modified couple-stress effect," *Composite Structures,* vol. 153, no. N/A, pp. 321-331, 2016.

[107] I. R. Clemitson, "5 Processing Fundamentals," in *Castable Polyurethane Elastomers*, Boca Raton, CRC Press, 2015, pp. 99-123.

[108] M. Serkis, M. Špírková, J. Kredatusová, J. Hodan and R. Bureš, "Organic–inorganic nanocomposite films made from polyurethane dispersions and colloidal silica particles," *Composite Interfaces,* vol. 23, no. 2, pp. 157-173, 2016.

[109] S. Yu, S. Yang and M. Cho, "Analysis of thermal conductivity of polymeric nanocomposites under mechanical loading," *Journal of Applied Physics,* vol. 114, no. 21, p. 213503, 2013.

[110] M. Bhattacharya, "Polymer Nanocomposites--A Comparison between Carbon Nanotubes,

Graphene, and Clay as Nanofillers," *Materials,* vol. 9, no. 4, pp. 1-35, 2016.

[111] I. H. Tseng, J. C. Chang, S. L. Huang and M. H. Tsai, "Enhanced thermal conductivity and dimensional stability of flexible polyimide nanocomposite film by addition of functionalized graphene oxide," *POLYMER INTERNATIONAL,* vol. 62, no. 5, pp. 827-835, 2013.

[112] W.-b. Zhang, X.-l. Xu, J.-h. Yang, T. Huang, N. Zhang, Y. Wang and Z.-w. Zhou, "High thermal conductivity of poly(vinylidene fluoride)/carbon nanotubes nanocomposites achieved by adding polyvinylpyrrolidone," *Composites Science & Technology,* vol. 106, no. N/A, pp. 1-8, 2015.

[113] XGSciences, *xGNP-M Data Sheet,* Lansing: XGSciences, 2013.

[114] A. Agrawal and A. Satapathy, "Mathematical model for evaluating effective thermal conductivity of polymer composites with hybrid fillers," *International Journal of Thermal Sciences,* vol. 89, no. N/A, pp. 203-209, 2015.

[115] J. Bouchard, A. Cayla, E. Devaux and C. Campagne, "Electrical and thermal conductivities of multiwalled carbon nanotubes-reinforced high performance polymer nanocomposites," *Composites Science & Technology,* vol. 86, no. N/A, pp. 177-184, 2013.

[116] A. J. Paleo, X. Garca, L. Arboleda-Clemente, F. W. Van Hattum, M. J. Abad and A. Ares, "Enhanced thermal conductivity of rheologically percolated carbon nanofiber reinforced polypropylene composites," *POLYMERS FOR ADVANCED TECHNOLOGIES,* vol. 26, no. 4, pp. 369-375, 2015.

[117] H. T. a. G. Srivastava, "Lattice Dynamics of Solids, Surfaces, and Nanostructures," in *Length-Scale Dependent Phonon Interactions*, New York, Springer Science, 2014, pp. 1-40.

[118] S. Hida, T. Hori, T. Shiga, J. Elliot and J. Shiomi, "Thermal Resistance and Phonon Scattering at the Interface Between Carbon Nanotube and Amorphous Polyethylene,"

International Journal Heat and Mass Transfer, vol. 67, pp. 1024-1029, 2013.

[119] Normac Adhesives, "NR-606," Normac Adhesives, [Online]. Available: http://www.normacadhesives.com/en/normac-products/castable/nr-606.html. [Accessed 4 February 2017].

[120] V. Causin, "Characterization of Nanocomposites by Scattering Methods," in *Polymer Composites: Volume 2*, Weinheim, Wiley-VCH, 2013, pp. 75-116.

[121] Hot Disk AB, *Hot Disk Thermal Constants Analyser Instruction Manual,* Fredricton: Hot Disk AB, 2013.

[122] Y. He, "Rapid thermal conductivity measurement with a hot disk sensor: Part 1. Theoretical considerations," *Thermochimica Acta,* vol. 436, no. 1-2, pp. 122-129, 2005.

[123] Hot Disk AB, *TPS-QSG-3 - Quick Start Guide - Anisotropic Method for the TPS System,* Fredricton: Hot Disk AB, 2014.

[124] ASTM International, *ASTM E1269-11, Standard Test Method for Determining Specific Heat Capacity by Differential Scanning Calorimetry,* West Conshohocken: ASTM International, 2011.

[125] W. Lin, "Modeling of Thermal Conductivity of Polymer Nanocomposites," in *Modeling and Prediction of Polymer Nanocomposite Properties*, Weinheim, Wiley-VCH, 2013, pp. 169-200.

[126] H. Zhou, S. Zhang and M. Yang, "The effect of heat-transfer passages on the effective thermal conductivity of high filler loading composite materials," *Composites Science & Technology,* vol. 67, no. 6, pp. 1035-1040, 2007.

[127] D. Bigg, "Thermal Conductivity of Heterophase Polymer Compositions," *Advances in Polymer Science,* vol. 119, pp. 1-30, 1995.

[128] S. Okamoto and H. Ishida, "A New Theoretical Equation for Thermal Conductivity of Two-Phase Systems," *Journal of Applied Polymer Science,,* vol. 72, pp. 1689-1697, 1999.

[129] A. Goswami, A. K, N. Balashanmugam, A. M. Umarji and G. Madras, "Optimization of rheological properties of photopolymerizable alumina," *Ceramics International,* vol. 40, p. 3655–3665, 2014.

[130] N. K. Anifantis, S. K. Georgantzinos, G. I. Giannopoulos and P. A. Kakavas, "Elastomer Macrocomposites," in *Advances in Elastomers II Composites and Nanocomposites*, Berlin, Springer, 2013, pp. 11-68.

APPENDIX

Averaged WAXD plots for the neat PU polymer, GNP powder, and PU-GNP nanocomposite at various filler loadings are presented in the following pages.

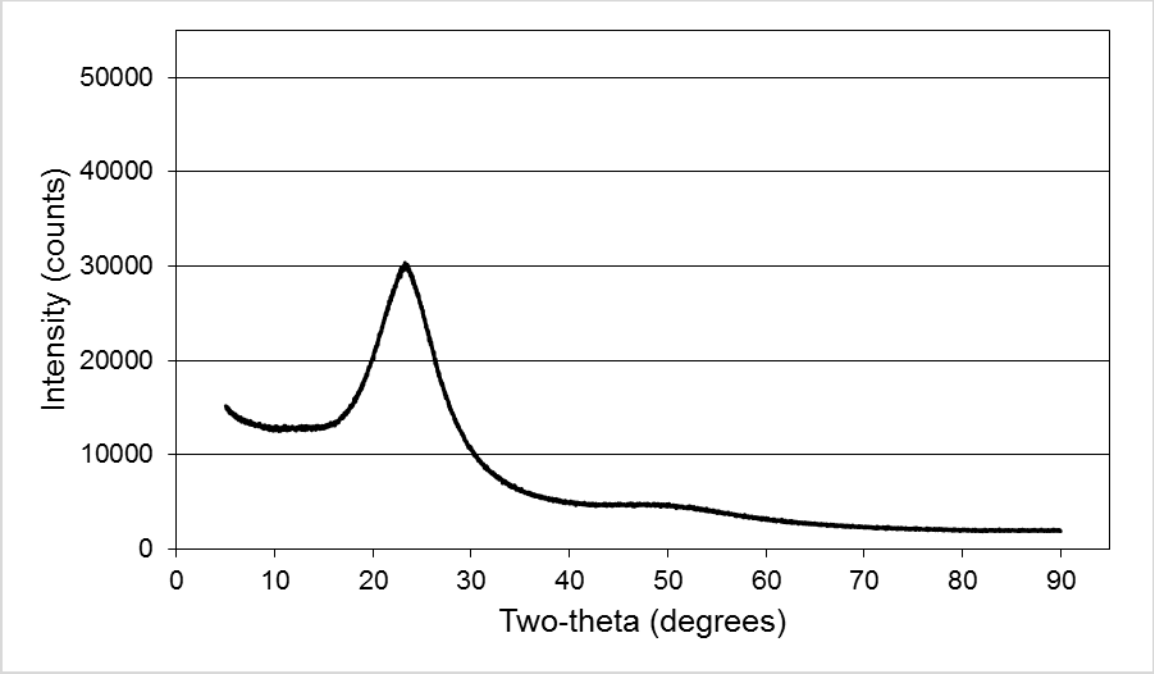

Figure 33 WAXD plot for the neat PU polymer

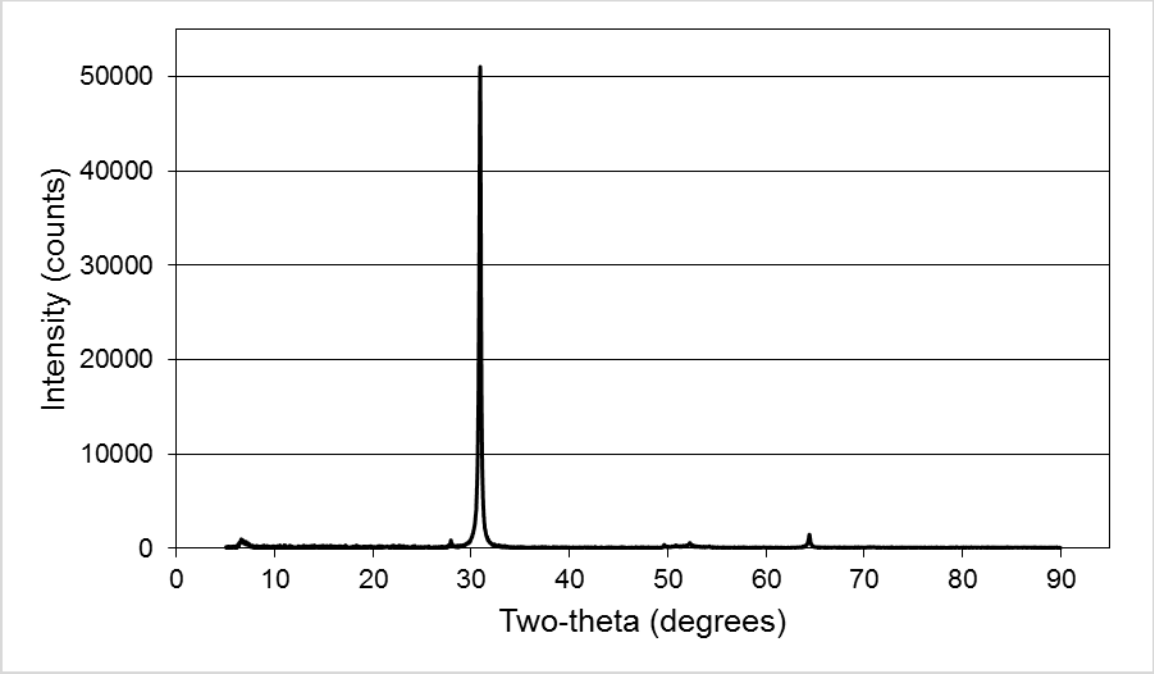

Figure 34 WAXD plot for the GNP bulk dry powder

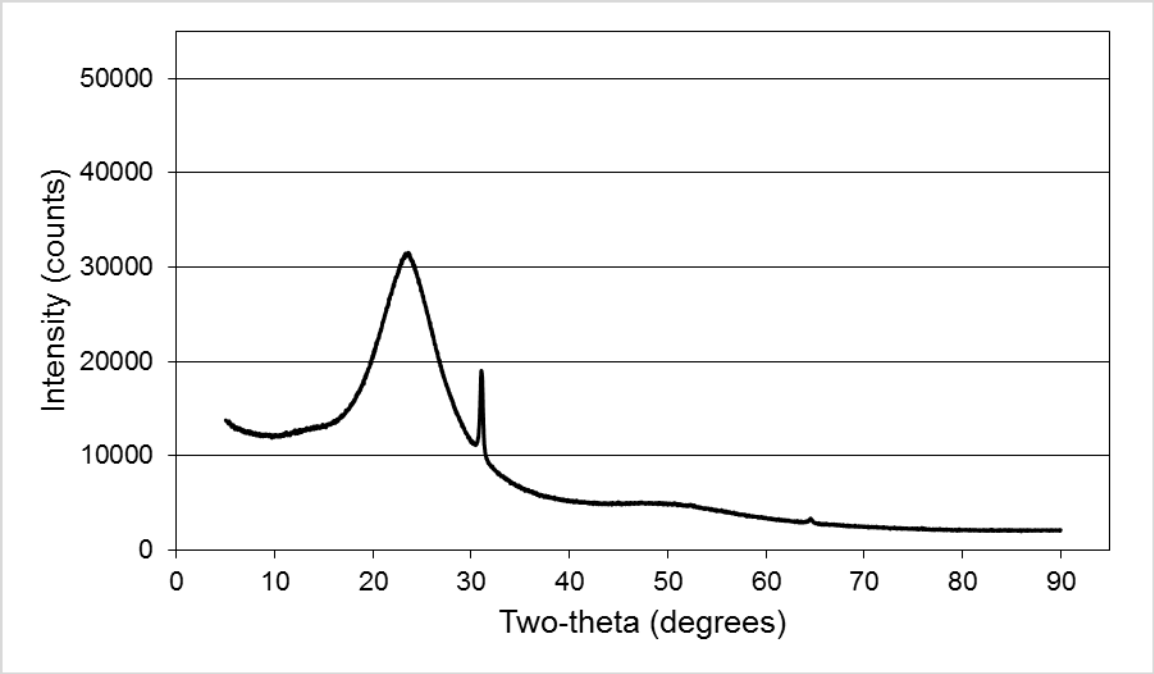

Figure 35 WAXD plot for 1% filler weight modified GNP-PU nanocomposite

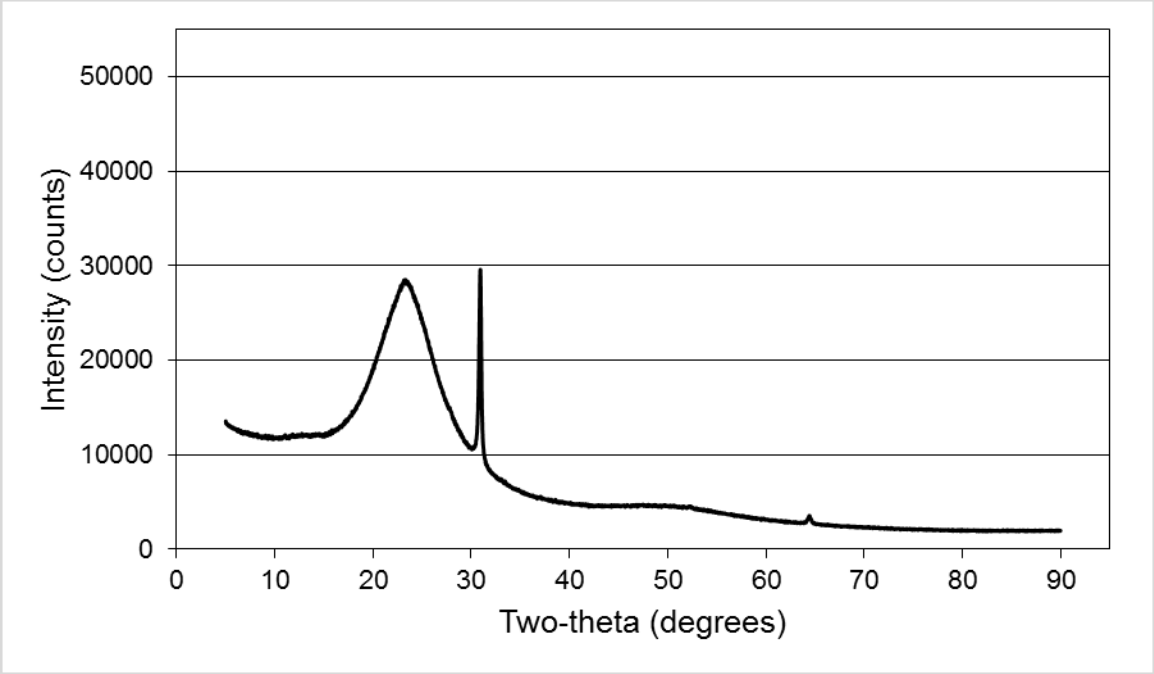

Figure 36 WAXD plot for 2% filler weight modified GNP-PU nanocomposite

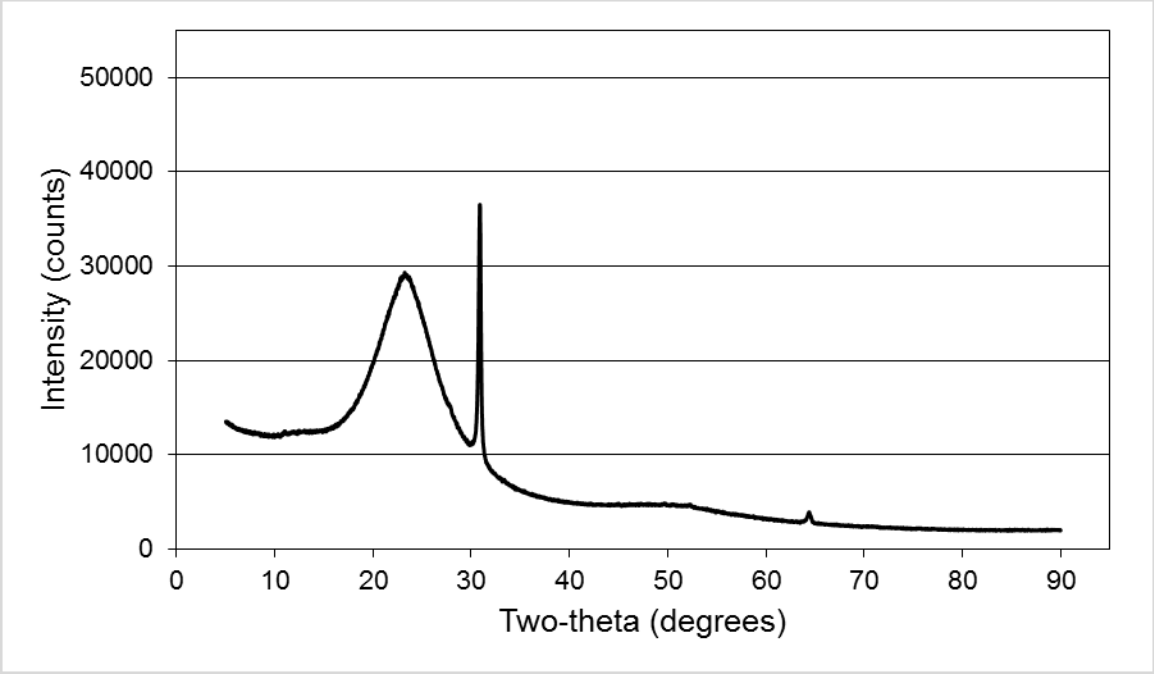

Figure 37 WAXD plot for 3% filler weight modified GNP-PU nanocomposite

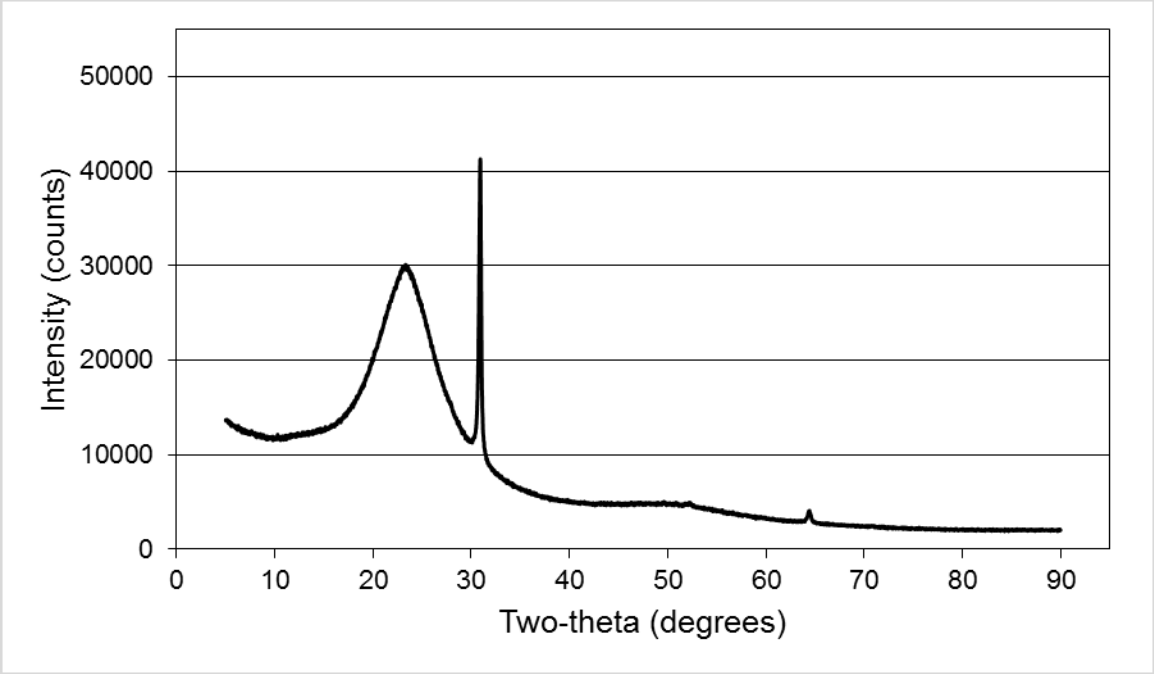

Figure 38 WAXD plot for 4% filler weight modified GNP-PU nanocomposite